Immunity

Antibody-Fab and -Fc features promote *Mycobacterium tuberculosis* restriction

Graphical abstract

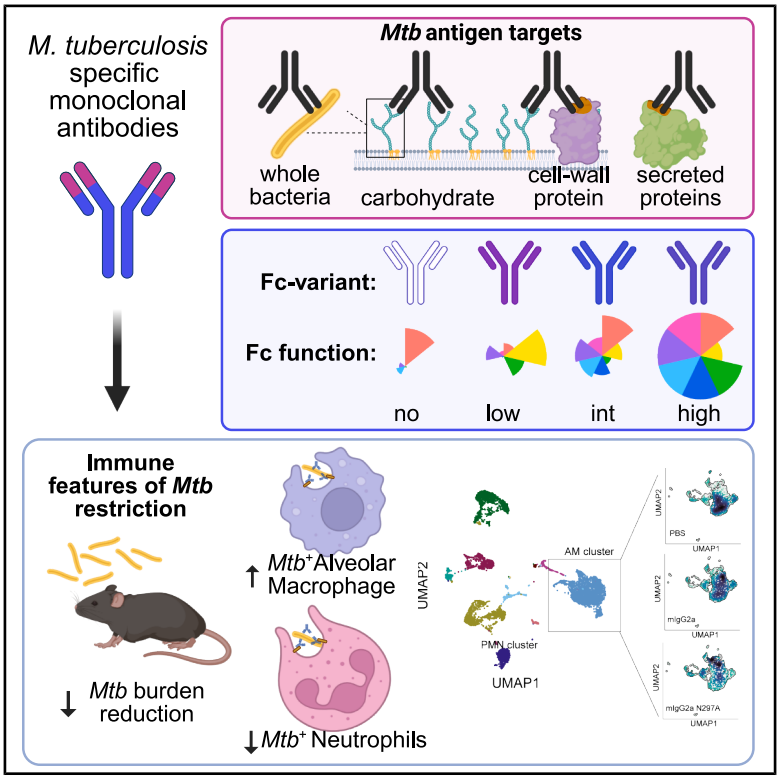

Authors

Patricia S. Grace, Joshua M. Peters, Jaimie Sixsmith, ..., Bryan D. Bryson, Sarah M. Fortune, Galit Alter

Correspondence

sfortune@hsph.harvard.edu (S.M.F.), galter@partners.org (G.A.)

In brief

Polyclonal *Mycobacterium tuberculosis*-specific antibody-mediated effector functions correlate with improved infection in humans; however, the precise antibody specificities and functions that contribute to this control remain undefined. Grace et al. employ an Fc-swapped monoclonal antibody screen to define the antigen specificity and functions that contribute to antimicrobial control *in vivo*.

Highlights

- Distinct *Mycobacterium tuberculosis*-specific antibodies restrict bacterial growth *in vivo*
- Fc-mediated functions contribute to antibody-mediated *M. tuberculosis* control
- Antibody Fc drives *M. tuberculosis* redistribution in innate immune cells of the lung
- Transcriptomic analysis reveals differential Fc-mediated immune cell activation

Grace et al., 2025, Immunity *58*, 1586–1597
June 10, 2025
https://doi.org/10.1016/j.immuni.2025.05.004

CellPress

CellPress
OPEN ACCESS

Immunity

Article

Antibody-Fab and -Fc features promote *Mycobacterium tuberculosis* restriction

Patricia S. Grace,[1,2] Joshua M. Peters,[1,3] Jaimie Sixsmith,[2] Richard Lu,[1] Edward B. Irvine,[1,2] Corinne Luedeman,[1] Brooke A. Fenderson,[1] Andrew Vickers,[2] Matthew D. Slein,[1] Tanya McKitrick,[4] Mo-Hui Wei,[4] Richard D. Cummings,[4] Aaron Wallace,[5] Lisa A. Cavacini,[5] Alok Choudhary,[6] Megan K. Proulx,[7] Christopher Sundling,[8,9] Gunilla Källenius,[8,9] Rajko Reljic,[10] Joel D. Ernst,[11] Arturo Casadevall,[12] Camille Locht,[13] Abraham Pinter,[6] Christopher M. Sassetti,[7] Bryan D. Bryson,[1,3] Sarah M. Fortune,[1,2,*] and Galit Alter[1,14,*]

[1]Ragon Institute of MGH, MIT, and Harvard, Cambridge, MA, USA
[2]Department of Immunology and Infectious Disease, Harvard T.H. Chan School of Public Health, Boston, MA, USA
[3]Department of Biological Engineering, Massachusetts Institute of Technology, Cambridge, MA, USA
[4]Department of Surgery, Beth Israel Deaconess Medical Center, Harvard Medical School, Boston, MA, USA
[5]MassBiologics of the University of Massachusetts Medical School, Boston, MA, USA
[6]Public Health Research Institute, New Jersey Medical School, Rutgers, The State University of New Jersey, Newark, NJ, USA
[7]Department of Microbiology and Physiological Systems, University of Massachusetts Medical School, Worcester, MA, USA
[8]Division of Infectious Diseases, Department of Medicine Solna and Center for Molecular Medicine, Karolinska Institute, Stockholm, Sweden
[9]Department of Infectious Diseases, Karolinska University Hospital, Stockholm, Sweden
[10]Institute for Infection and Immunity, St. George's University, London, UK
[11]Division of Experimental Medicine, University of California, San Francisco, San Francisco, CA, USA
[12]Department of Molecular Microbiology and Immunology, Johns Hopkins Bloomberg School of Public Health, Baltimore, MD, USA
[13]University of Lille, CNRS, Inserm, CHU Lille Institut Pasteur de Lille, U1019-URM9017_Center for Infection and Immunity of Lille, 5900 Lille, France
[14]Lead contact
*Correspondence: sfortune@hsph.harvard.edu (S.M.F.), galter@partners.org (G.A.)
https://doi.org/10.1016/j.immuni.2025.05.004

SUMMARY

Mycobacterium tuberculosis, the causative agent of tuberculosis (TB), a leading cause of death by an infectious disease globally, has no efficacious vaccine. Antibodies are implicated in *M. tuberculosis* control, but the mechanisms of action remain poorly understood. We assembled a library of monoclonal antibodies (mAb) and screened for *M. tuberculosis*-restrictive activity in mice, identifying protective antibodies targeting diverse antigens. To dissect the mechanism of mAb-mediated *M. tuberculosis* restriction, we optimized a protective lipoarabinomannan-specific mAb, generating Fc variants. *In vivo* analysis of these Fc variants revealed a role for Fc-effector function in *M. tuberculosis* restriction. Restrictive Fc variants altered distribution of *M. tuberculosis* across innate immune cells. Single-cell transcriptomics highlighted distinctly activated pathways within innate immune cell subpopulations, identifying early activation of neutrophils as a key signature of mAb-mediated *M. tuberculosis* restriction. Therefore, antibody-mediated restriction of *M. tuberculosis* is associated with reorganization of the tissue-level immune response to infection and depends on the collaboration of antibody Fab and Fc.

INTRODUCTION

With an estimated 10 million new cases worldwide and approximately 1.6 million associated deaths annually, tuberculosis (TB) remains one of the world's deadliest infectious diseases.[1] Novel drugs, host-directed therapies, and vaccines are needed to combat this global health threat. While cell-mediated immunity is critical for limiting intracellular *Mycobacterium tuberculosis* infection,[2] recent data suggest the importance of humoral responses in mediating control. Humoral immunity has been relatively understudied in TB, but passive transfer of intravenous immunoglobulin (IVIG),[3,4] antibodies from TB patients,[5,6] and vaccine-induced antibodies[7] in mice demonstrate that antibodies can promote *M. tuberculosis* restriction, although these effects vary between studies.[8] Similarly, monoclonal antibodies (mAbs) targeting *M. tuberculosis* cell wall-associated antigens lipoarabinomannan (LAM)[9,10] and heparin-binding hemagglutinin (HBHA),[11] as well as those targeting the membrane-associated PstS1[12] and intracellular protein HspX,[13] have been shown to protect animals against *M. tuberculosis* challenge. However, it remains unclear how antibodies mediate *M. tuberculosis* infection control.

Antibody function is governed not only by antigen specificity, conferred by the antigen-binding (Fab) domain to neutralize pathogens but also by the antibody constant (Fc) domain, which recruits complement and engages Fc receptors (FcRs) on the

Table 1. TB mAb clones and antigen targets

mAb clone	Antigen	Reference
712	Ag85B	Ernst et al.[27]
710	Ag85B	Ernst et al.[27]
CS-90	Ag85 complex	BEI Resources
CP2-R19	ESAT6/CFP10	see Table S1and Figures S1and S2
a-Rv1411c	LprG	BEI Resources
D2	HBHA	Pethe et al.[11]
Apa 30	Apa	–
CP2-LR5	PstS1	see Table S1and Figures S1and S2
IT-15	PhoS1/PstS1	BEI Resources, Foreman et al.[29]
Mpt64(B)	Mpt64	BEI Resources
2e9	HspX	Balu et al.[13]
OM2-L2	HspX	see Table S1and Figures S1and S2
KatG2	KatG	BEI Resources, Foreman et al.[29]
C1-LR/NP12	unknown	see Table S1and Figures S1and S2
CP2-LR17	capsule polysaccharides/ lipopolysaccharides	see Table S1 and Figures S1 and S2
24c5	alpha-glucan	Teitelbaum et al.[10]
CP2-R3	glycopeptidolipids	see Table S1 and Figures S1 and S2
OM2-L7	glycopeptidolipids	see Table S1 and Figures S1 and S2
OM2-L22	glycopeptidolipids	see Table S1 and Figures S1 and S2
SMITB14	LAM (AM)	Hamasur et al.[9]
A194	LAM	Choudhary et al.[28]
MoAb1	LAM (MTX)	Choudhary et al.[28]
CS-35	LAM	BEI Resources, Chatterjee et al.[26]
OM2-R18	inner membrane and intracellular peptide glycans	see Table S1 and Figures S1 and S2

surface of immune cells. These interactions promote Fc-effector functions including phagocytosis, cellular cytotoxic responses in natural killer (NK) cells, and macrophage activation.[14,15] The mere presence of *M. tuberculosis*-specific antibody titers in a host does not guarantee protection against infection or disease.[8] Instead, emerging data suggest that antibody Fc-effector functions, diverge across TB disease states, and may better predict antibody-mediated protection.[16] Recently, humoral immune responses have been linked to reduced rates of infection in a TB vaccination study in humans[17] as well as in non-human primates.[18] Mice lacking the Fc gamma chain (Fcγ chain), the FcR moiety key to intracellular signaling and function, exhibit a diminished capacity to restrict *M. tuberculosis*, compared with wild-type (WT) mice,[19] indicating that immunoglobulin G (IgG) interactions with FcR contributes to immune control of infection. Consistent with this, point mutations of the IgG Fc domain, which reduce FcR engagement of protective mAbs, eliminated antibody-mediated *M. tuberculosis* restriction.[12,20] Further, *M. tuberculosis*-specific Fabs generated with IgA and IgM Fc domains exhibit increased *M. tuberculosis*-restrictive capacity *in vitro*,[18,21] emphasizing that Fc-effector function is also important for antimicrobial activity of antibodies during *M. tuberculosis* infection. However, it is unclear whether antibodies to diverse antigens or even distinct epitopes within the same antigen confer protection, and how Fc-effector functions contribute to *M. tuberculosis* restriction *in vivo* is unknown.

To investigate the role of antibody Fab and Fc in immune-mediated *M. tuberculosis* restriction, we profiled the largest library of *M. tuberculosis*-specific mAbs to date for the ability to drive bacterial control in mice. Screening this library, we identified diverse antigen targets of mAbs able to restrict *M. tuberculosis* growth *in vivo*, which were not predicted by antibody opsonization. A protective LAM-specific mAb with swapped Fc domains and varying Fc-effector functions revealed that antibody Fc contributes to antibody-mediated *M. tuberculosis* restriction. The most functional Fc variant (mIgG2a) of the αLAM-mAb exhibited enhanced restriction of *M. tuberculosis* in mice. Treatment of mice with the mIgG2a Fc variant prior to infection altered *M. tuberculosis* tropism for different innate immune cell populations in the lung. Single-cell transcriptional profiling of lung innate immune cells pointed to distinct pathway activation in alveolar macrophages (AMs) and neutrophils in the presence of the restrictive αLAM-mIgG2a at initial stages of *M. tuberculosis* infection. These data suggest that protective antibodies cooperate with the innate immune response, rewiring interactions of *M. tuberculosis* with innate immune cells within the lung.

RESULTS

Both *M. tuberculosis*-opsonizing and non-opsonizing mAbs promote *M. tuberculosis* restriction *in vivo*

M. tuberculosis expresses an array of protein and glycolipid antigens, which is targeted by antibody responses in humans,[22,23] and passive transfer of these antibodies to *M. tuberculosis*-infected mice suggests that some polyclonal pools harbor protective antigen-specific antibodies.[3,5,6,24] The transfer of mAbs specific for a limited number of antigen targets is described to give rise to various *M. tuberculosis* control phenotypes: restricting bacterial replication in the lung, preventing spleen dissemination, or increasing animal survival.[9,11–13,25] Despite this evidence, the identity of the many potential *M. tuberculosis*-antigen targets or even epitopes within an individual antigen that can promote *M. tuberculosis* restriction in the lung remains incompletely characterized. Many studies have focused on the protection mediated by antibodies targeting surface-associated glycan and protein antigens. Whether antibodies targeting intracellular or secreted antigens provide protection equivalent to these surface-associated targets is unclear. Thus, we generated a library of 24 mAbs, targeting various *M. tuberculosis* antigens (Table 1) to identify antigens targeted by antibodies that could promote antimicrobial activity in mice,[26] including mAbs previously described to confer varying protective *M. tuberculosis* phenotypes in mice.[9–11,13,27–29] Additionally, we screened mAbs derived from vaccination against capsular (CP) and outer membrane (OM)

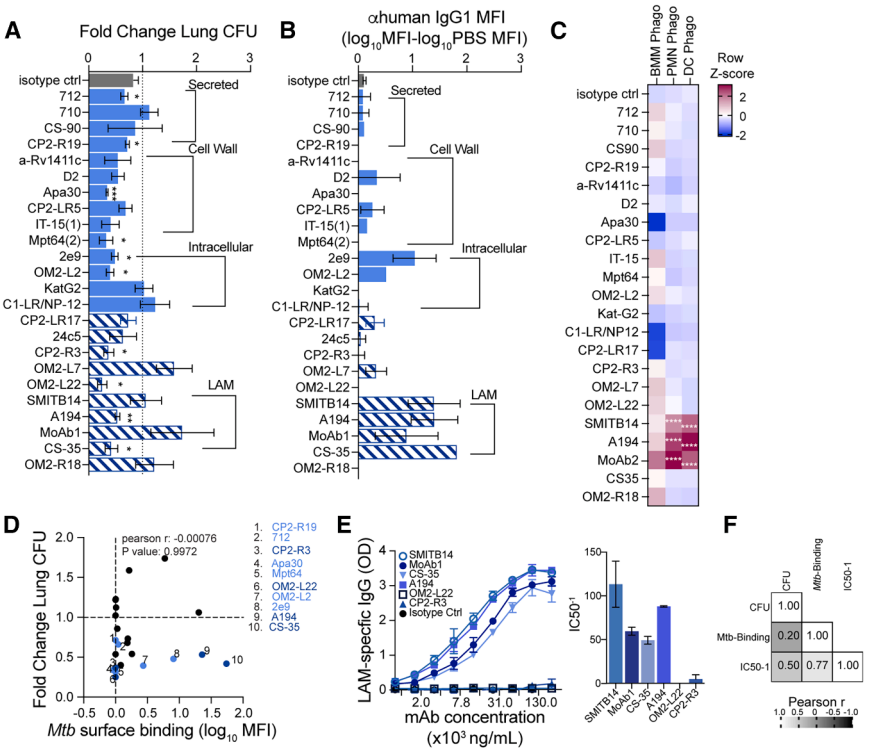

Figure 1. Passive transfer screen of mAbs in mice identifies protein- and glycolipid-binding antibodies that restrict *M. tuberculosis* growth

A library of human IgG1 (hIgG1) monoclonal antibodies (mAbs) targeting proteins (solid light blue bars) and glycolipid antigens (hashed navy bars) was screened for *M. tuberculosis* growth restriction in mice along with a hIgG1 isotype control antibody (gray bar). C57BL/6 mice were pretreated with 100 μg of mAb and infected via aerosol with ~100 day 1 CFUs of *M. tuberculosis*, and brackets denote class/localization of TB antigen targets for each mAb clone. Table 1 defines these antigen targets in more detail.

(A) Fold change of lung colony-forming units (CFUs) of mAb-treated mice determined by division of mAb-treated mouse CFUs by average CFUs of control mice (PBS) in each round of infection (linear scale). Data are representative of 2 independent experiments (n = 3 mice). Graphs depict the mean ± SEM, and mAb mediating significant restriction was identified by one sample t test: $^{*}p < 0.05$, $^{**}p < 0.01$, $^{***}p < 0.005$.

(B) Bar plots represent fold enrichment of hIgG1 MFI on the surface of *M. tuberculosis* measured for each monoclonal via flow cytometry. Signal is background subtracted.

(C) Fluorescent *M. tuberculosis* and mAb were combined prior to exposure to mouse DC-, neutrophil-, and macrophage-derived bone marrow (see also Figure S2A). Heatmap depicts the phago scores calculated, which were Z scored per cell type tested. Data are representative of 2 independent experiments (n = 2 replicates). mAb clones that significantly enhanced *M. tuberculosis* phagocytosis were identified by one-way ANOVA: $^{****}p < 0.0001$.

(D) *M. tuberculosis* surface binding plotted against lung CFUs are poorly correlated. *M. tuberculosis*-restrictive protein-specific mAbs (light blue) and glycolipid-specific mAbs (dark blue).

(E) Relative mAb binding measured by LAM ELISA. The inverse IC50 describes the binding capacity of each mAb. Data are representative of 2 independent experiments.

(F) Pearson correlation r of LAM-binding mAbs with *M. tuberculosis* surface-binding and LAM-binding $IC50^{-1}$. See also Table S1 and Figures S1 and S2.

fractions of *M. tuberculosis*. These CP and OM mAbs were characterized to determine *M. tuberculosis* antigen binding (Table S1; Figure S1). For consistency and comparability, the Fab domain of each mAb was produced with a human IgG1 (hIgG1) Fc domain, known to interact with FcR and to mediate Fc-effector functions in mouse immune cells.[30] The mAb library was screened in mice to identify mAbs that mediated *M. tuberculosis* growth restriction *in vivo*. Ten antibodies promoted significant fold reduction of *M. tuberculosis* colony-forming units (CFUs), compared with PBS-treated mice (Figure 1A). Both protein- and glycolipid-specific antibodies restricted *M. tuberculosis in vivo*.

M. tuberculosis surface opsonization by antibodies has previously been associated with *M. tuberculosis* restriction *in vivo*.[6,31] Thus, we tested whether restrictive mAbs bound to *M. tuberculosis* more effectively than non-restrictive mAbs. A head-to-head comparison of mAb binding was performed with live *M. tuberculosis*, revealing, as expected, that LAM-specific mAbs robustly opsonized *M. tuberculosis* (Figure 1B, hashed bars), while many of the protein-targeting mAbs did not (solid blue bars). Specifically, *M. tuberculosis* opsonization assay revealed negligible anti-human IgG Fc MFI associated with mAbs targeting secreted proteins (Ag85B, clone 712) and variable binding for cell wall protein-specific or intracellular protein-specific mAbs (e.g., Apa, clone Apa30 and HspX, clones 2e9 and OM2-L2) (Figure 1B).

Previous studies found a correlation between mAb opsinophagocytic activity and bacterial restriction.[31,32] We tested these mAbs for the ability to increase bacterial phagocytosis in mouse macrophages, neutrophils, and dendritic cells (DCs). LAM-specific mAbs promoted significant increases in *M. tuberculosis* phagocytosis (phago score) in DCs and neutrophils, compared with isotype control treatment, but no significant antibody-mediated increases in *M. tuberculosis* uptake were observed in macrophages (Figures 1C and S2A). We found a moderate correlation between *M. tuberculosis* surface binding and *M. tuberculosis* phagocytosis in DCs and neutrophils, suggesting that antibody opsonization can enhance bacterial uptake by these cells (Figure S2B). However, when comparing across this library, there was no significant correlation between phagocytic function and *in vivo* control (Figure S2B). These results indicate that both opsonizing and non-opsonizing antibodies can promote *M. tuberculosis* restriction *in vivo*.

The degree of *M. tuberculosis* surface binding did not correlate with *in vivo* restriction (Figure 1D). Specifically, not all antibodies targeting the surface-abundant LAM antigen restricted *M. tuberculosis* outgrowth *in vivo*. Instead, the LAM-specific clones promoted highly variable *M. tuberculosis* growth phenotypes from restriction to near enhancing effects in mice. To further dissect the determinants of LAM-specific *in vivo* restriction, we

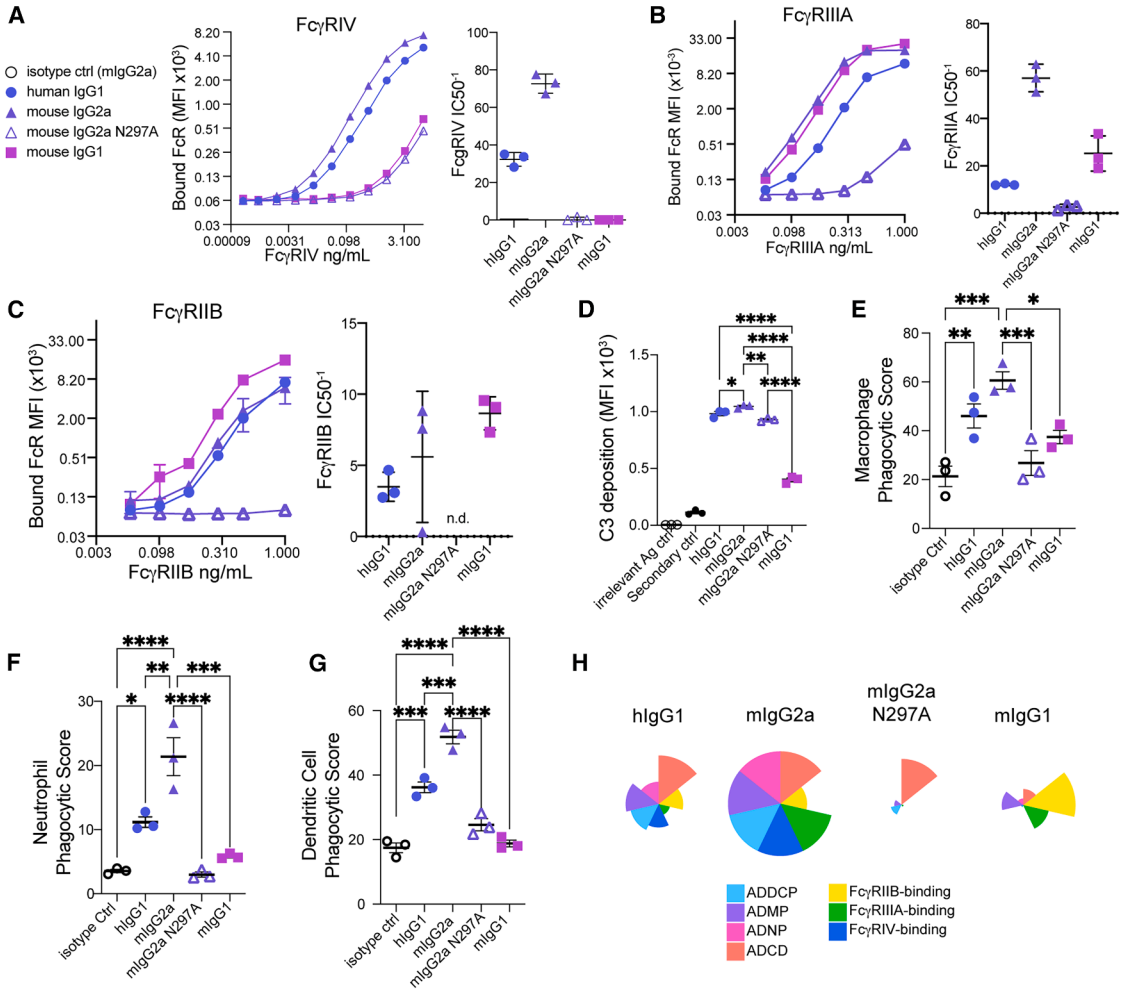

Figure 2. FcR-binding and Fc-effector functions of αLAM Fc variants

(A–C) Luminex beads were combined with Fc-variant mAbs to test for the ability to bind mouse FcRs. Graphs depict MFI of (A) PE-FcγRIV, (B) -FcγRIIIA, and (C) -FcγRIIB bound to LAM beads complexed with αΛΑΜ (A194) Fc variants; n.d., not detected.

(D–G) (D) Relative MFI of αC3-fluorescein isothiocyanate (FITC) antibody used to detect complement C3 deposition on LAM-bead immune complexes (IC). Phagocytic scores determined for αLAM Fc variant-opsonized *M. tuberculosis* in bone marrow-derived (E) macrophages, (F) neutrophils, and (G) DCs.

Data are representative of 2 independent experiments. Graphs depict the mean ± SEM. Significant differences between Fc variants were determined by one-way ANOVA with Tukey's multiple correction: *p, 0.05; **p, 0.01; ***p, 0.005.

measured the binding affinity of the LAM-specific mAbs for the cognate LAM antigen. We found no significant differences in binding affinity across the LAM-specific mAbs (Figure 1D). While affinity weakly correlated with *M. tuberculosis* surface binding, antigen-specific affinity did not correlate with the growth restriction observed in mice (Figure 1E). Collectively, profiling this large mAb library indicates that not only high affinity opsinophagocytic antibodies restrict *M. tuberculosis* growth, but that antibodies targeting secreted, cell wall-associated, or canonically intracellular proteins can promote *M. tuberculosis* restriction *in vivo*.

Fc domain swapping of an αLAM mAb enhances antibody-mediated effector function

Previous data point to a role for antibody cooperation with the innate immune system, via Fc-effector functions, as a key mechanism in the control of *M. tuberculosis*. To dissect the impact of Fc-effector function on *M. tuberculosis* control *in vivo* we focused on the LAM-specific mAb clone A194,[28] which displayed restrictive efficacy *in vivo* and enhanced phagocytic function in our screen. We reasoned that swapping the Fc domain of this αLAM mAb for specific mouse isotypes would modulate Fc-effector function and might impact the restrictive effect of the LAM-specific mAb. In addition to the hIgG1 variant that we screened previously, we generated a functional mouse IgG2a (mIgG2a) Fc variant, an FcR-binding knockout mIgG2a N297A point mutant, and a mouse IgG1 (mIgG1) Fc variant. We assayed FcR binding and antibody effector functions of the αLAM Fc variants complexed with LAM-coated beads or *M. tuberculosis*. Consistent with previous reports,[30,33] the mIgG1 and mIgG2a N297A Fc variants displayed negligible binding to the activating FcγRIV receptor, while the hIgG1 and mIgG2a variants bound with high affinity (Figure 2A). The mIgG2a, mIgG1, and hIgG1

variants bound with decreasing strength to FcγRIIIA, while the mIgG2a N297A displayed no apparent binding (Figure 2B). Finally, the mIgG1 variant bound with the greatest affinity to FcγRIIB; the mIgG2a and hIgG1 bound with relatively moderate affinity, while the mIgG2a N297A had no apparent binding to FcγRIIB (Figure 2C).

Differences in FcR affinity impart differential Fc-effector function.[30] In addition to biophysical measures of FcR interactions, we compared the capacity of Fc variants to mediate complement recruitment and *M. tuberculosis*-phagocytic functions. When the mAbs were complexed with LAM-coated beads, all Fc variants were able to recruit C3 complement on immune complexes, indicating mature complement-complex formation, but the mIgG1 variant immune complex recruited less C3 (Figure 2D). Notably, while the mIgG2a N297A displayed reduced FcR interactions, the ability of the variant to recruit complement was maintained. We also screened Fc-mediated phagocytic function in murine macrophages, neutrophils, and DCs and found that the mIgG2a variant possessed enhanced phagocytic activity in macrophages (Figure 2E), neutrophils (Figure 2F), and DCs, when compared with the hIgG1 variant (Figure 2G). As expected, the FcR-binding mutant mIgG2a N297A had no appreciable phagocytic capacity, compared with an isotype control antibody, in any of the cell types tested. The mIgG1 variant displayed modest phagocytic capacity when compared with the mIgG2a Fc variant. Across the biophysical and functional measures, we confirmed that swapping the Fc domains altered the functional capacity of the αLAM mAb, with each variant displaying distinct FcR and cellular engagement patterns (Figure 2H).

αLAM-Fc variants leverage distinct cellular immune responses *in vivo* during *M. tuberculosis* infection

The diverse functional profiles of the Fc variants provided an opportunity to probe the role of Fc-effector function in modulating *M. tuberculosis* infection *in vivo*. We selected the enhanced (mIgG2a), intermediate (mIgG1), and reduced (mIgG2a N297A) Fc variants to investigate Fc-mediated immune responses to *M. tuberculosis* infection. Fc variants were passively transferred into mice, and animals were challenged with low-dose aerosolized *M. tuberculosis*. Following infection, we tracked how immune responses changed across the distinct Fc variant-treated groups. Using multi-parameter flow cytometry, we tracked immune cell recruitment and fluorescent *M. tuberculosis* distribution among AMs, eosinophils, polymorphonuclear neutrophils (PMNs), classical Ly6C^{high} monocytes, non-classical monocytes (Ly6C^{low}FcgRIV^{high}),[34] interstitial macrophages (IMs), CD11b^{+} DCs, and CD103^{+} DCs recruited to the lung (Figure S3).[35,36] Analysis of lung cells 14 days post *M. tuberculosis* challenge revealed a shift in relative proportions of immune cells in the setting of specific Fc-variant treatments, compared with controls (Figure 3A), although the total number of myeloid cells was not statistically different across the treatment groups (Figure 3B). Specifically, we observed elevated AM numbers within the lungs of mice treated with mIgG2a and mIgG2a N297A Fc variants, compared with mice treated with mIgG1 or control mice (Figure 3C).

Using yellow fluorescent protein (YFP)-expressing *M. tuberculosis*, we also tracked *M. tuberculosis* distribution across lung immune cells. Consistent with previous reports in C57BL/6 mice 14 days post infection,[37,38] YFP-*M. tuberculosis* was found within AMs, PMNs, and IMs of all animals regardless of *M. tuberculosis* treatment (Figure 3D). However, the Fc variants differentially affected the relative distribution of *M. tuberculosis* among the three cell types. The mIgG2a-N297A treatment resulted in significantly higher numbers of *M. tuberculosis*+ immune cells (Mtb^{+}CD45^{+}) (Figure 3E) and greater relative numbers of *M. tuberculosis*+ AMs (Figure 3F), PMNs (Figure 3G), and RMs (Figure 3H), compared with treatment with any other Fc variants. These data suggest that loss of FcR engagement but retained complement recruitment activity (Figure 2D) may promote differential bacterial entry into immune cells. The effects of the other Fc variants were less pronounced, although mIgG2a treatment resulted in greater numbers of *M. tuberculosis*+ AMs (Figure 3F) and higher ratios of infected AMs to PMNs when compared with other Fc variant treatments (Figure 3I). These results indicate that mAbs with enhanced Fc-effector function promote residence of *M. tuberculosis* within AMs and may either limit *M. tuberculosis* uptake by or promote bacterial growth restriction within neutrophils.

αLAM mIgG2a treatment is associated with temporal bacterial restriction *in vivo*

We next determined the effect of the different αLAM Fc variants on bacterial restriction in the lungs of mice following *M. tuberculosis* aerosol challenge (Figure 4A). Treatment with the αLAM-mIgG2a Fc variants, like the hIgG1 screened previously (Figure 1A), resulted in significantly lower bacterial burden in the lung, when compared with that of control mice, 14 days post infection (Figure 4B). Conversely, no restriction was observed with mIgG2a-N297A, the Fc variant with reduced FcR binding, or the less functional mIgG1 Fc variant, indicating that Fc-effector function is required for αLAM-mediated bacterial control. *M. tuberculosis* dissemination from the lung to other tissues occurs in a non-linear fashion 11–17 days following infection[39]; notably, at the early time point of 14 days, we detected *M. tuberculosis* only within spleens of mIgG2a N297A-treated mice (Figure 4C). These data indicate that Fc-effector function is key to the αLAM-mediated restrictive effect on *M. tuberculosis*.

The effect of Fc-variant treatment changed over time. While the effect on *M. tuberculosis* restriction was evident 14 days post infection, there were no differences in lung CFUs across the treatment groups within the first week of infection (Figure 4D). Moreover, the effect of Fc-variant treatment on *M. tuberculosis* growth was no longer significant by 3 weeks post infection (Figure 4E), when passively transferred antibodies are reported to wane from circulation.[40,41] Collectively, these data are consistent with a model where the presence of an antibody capable of inducing strong Fc-effector functions promotes temporal *M. tuberculosis* restriction during the early stages of infection.

Fc variants mediate no appreciable *Mycobacterium tuberculosis* growth difference *in vitro*

Given the differences in bacterial outgrowth and the differential distribution of *M. tuberculosis* among immune cells that we observed in Fc-variant-treated mice, we measured the *in vitro* effect of Fc-variants on antibody-mediated *M. tuberculosis* growth restriction in specific lung immune cells. We focused on

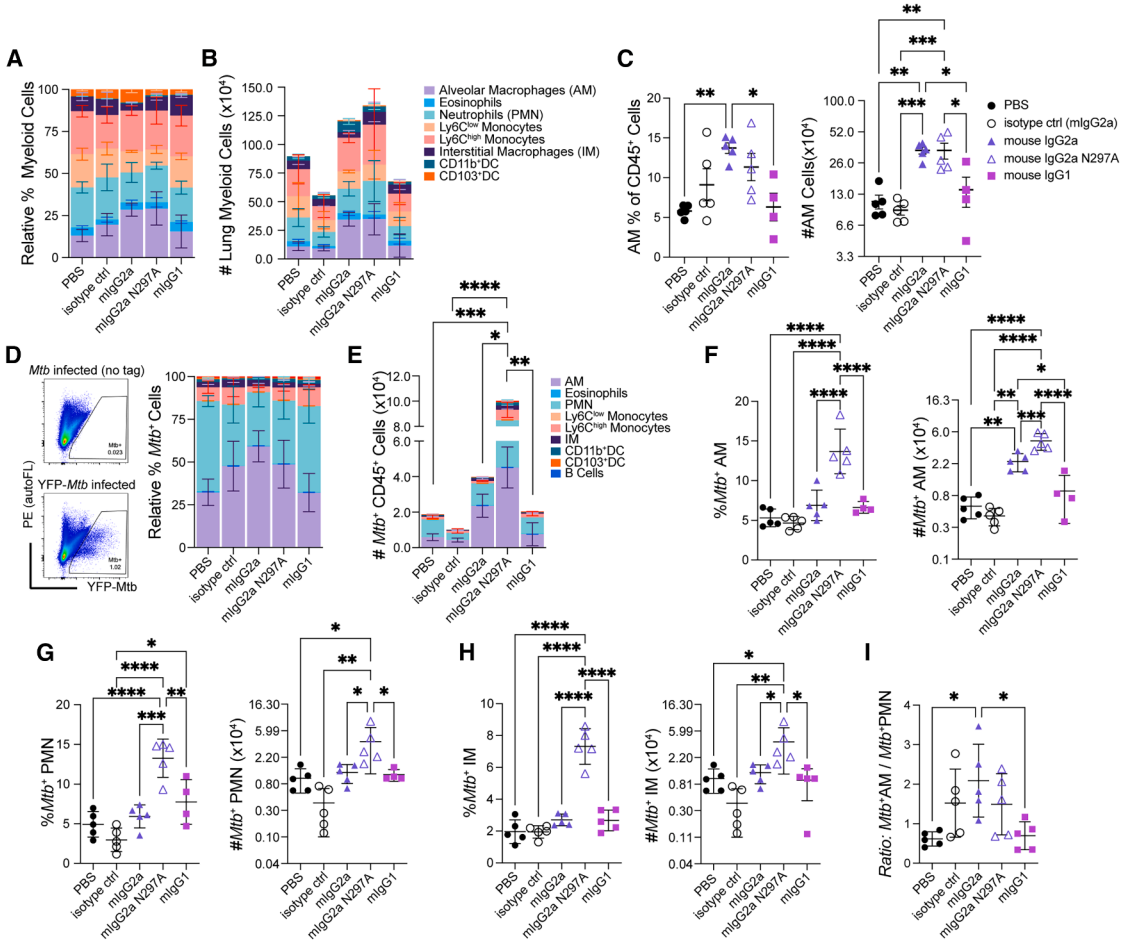

Figure 3. *M. tuberculosis* infection of AMs is enriched within αLAM mIgG2a-treated mice

(A and B) C57BL/6 mice were pre-treated with 100 μg of αLAM (A194) and infected via aerosol with ~100 day 1 *M. tuberculosis* CFUs. Single-cell suspensions of lung tissue from mAb-treated mice were generated and phenotypically analyzed using flow cytometry (see also Figure S3). Stacked bar plots show (A) relative frequency (%) of myeloid cell types and (B) total numbers (#) of myeloid cells by type present in the lung 14 days post infection.

(C) Frequency (%) and number (#) of alveolar macrophages (AMs).

(D) Flow plots depict YFP-*M. tuberculosis* signal detected in lung cells at 14 days, and bar plots show relative frequency of *M. tuberculosis*-infected cells by type.

(E) Total numbers of *M. tuberculosis*-infected cells by type.

(F) % and # of *Mtb*$^+$ AMs.

(G) % and # of *Mtb*$^+$ PMNs.

(H) % and # of *Mtb*+ IM.

(I) Ratio of *Mtb*$^+$ AM to *Mtb*$^+$ PMN. Data are representative of 2 independent experiments (n = 4–5 mice per treatment group).

Graphs depict the mean ± SEM, and significant differences between Fc variants were determined by one-way ANOVA with Tukey's multiple correction: *p, 0.05; **p, 0.01; ***p, 0.005; and ****p, 0.0001. See also Figure S3.

macrophages and neutrophils, which were the dominantly infected cell types in mouse lungs. We sorted AMs, IMs, and PMNs from the lungs of naive mice. We combined Fc-variants and luciferase-expressing *M. tuberculosis* (lux-*M. tuberculosis*), forming Fc-variant immune complexes, which we exposed to the sorted immune cells. We tracked *M. tuberculosis* outgrowth via luminescence over time and observed no Fc variant-mediated restriction of *M. tuberculosis* in the sorted AMs (Figure S4A), IMs (Figure S4B), and PMNs (Figure S4C). The lack of mAb-mediated *M. tuberculosis* restriction *in vitro* indicated a potential non-canonical mechanism of mAb-mediated bacterial restriction that was not observable using individually cultured cells.

Fc-dependent signaling in AM and neutrophil populations early in *Mycobacterium tuberculosis* infection

To evaluate how Fc function may shape immune signaling *in vivo* and bacterial control, we performed single-cell RNA sequencing (scRNA-seq) on lung immune cells from *M. tuberculosis*-infected mice treated with the restrictive αLAM mIgG2a variant, non-restrictive mIgG2a N297A variant, or PBS. We focused on cell state early during infection (5 days) to identify transcriptomic differences that are likely to contribute to, rather than result from, CFU differences observed 14 days post infection (Figure 5A).

As observed 1 week post infection (Figure 4D), *M. tuberculosis* burden in the lungs were similar in all treated animals 5 days

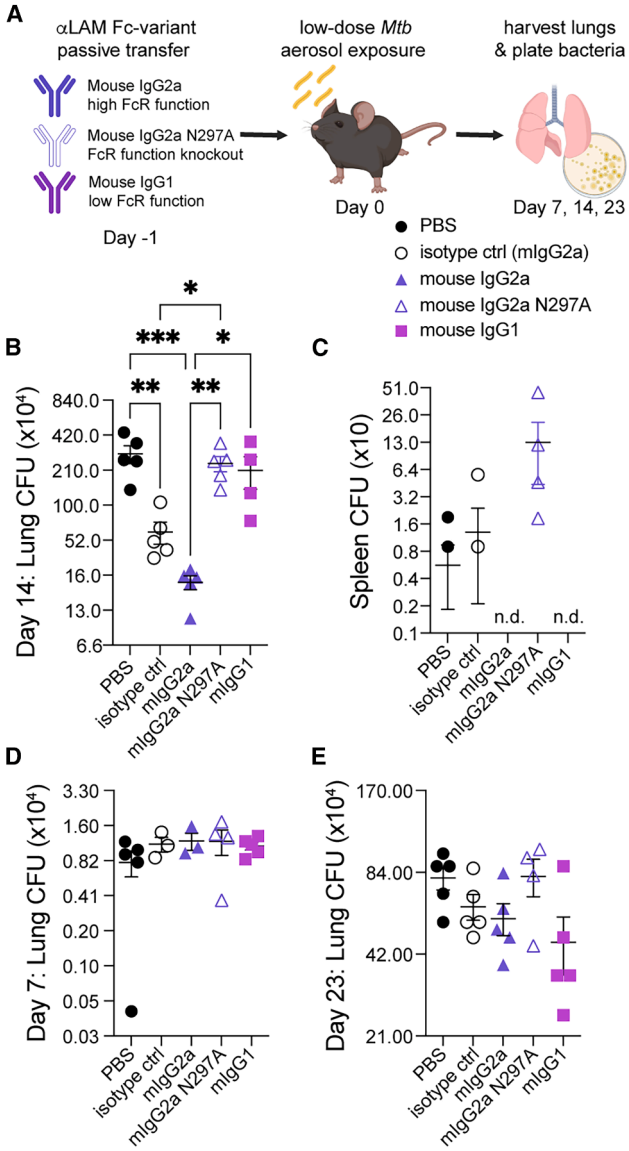

Figure 4. αLAM-mIgG2a restricts *M. tuberculosis* growth in early infection

(A–C) C57BL/6 mice were pre-treated with 100 μg of αLAM (A194) and infected via aerosol with ~100 day 1 *M. tuberculosis* CFUs.

(B and C) (B) Lung and (C) spleen CFUs were measured 14 days post infection in αLAM Fc variant-treated mice; n.d., not detected.

(D) Lung CFU 7 days post infection.

(E) Lung CFUs 23 days post infection. Data are representative of 2 independent experiments (n = 4–5 mice per treatment group). Graphs depict the mean ± SEM, and significant differences between Fc variants were determined by one-way ANOVA with Tukey's multiple correction: *p, 0.05; **p, 0.01; ***p, 0.005; ****p, 0.0001.

post infection (Figure S5A). We sorted Mtb+ and Mtb− CD45$^+$ cells from PBS-, αLAM-mIgG2a-, and -mIgG2a N297A-treated mice (n = 3 mice per treatment) for scRNA-seq, recovering 6,702 CD45+ cells from all mice in all conditions. Eleven distinct cell populations were identified by transcriptomic clustering,[42] including neutrophils, AMs, myeloid cells, NK cells, B cells, monocytes, plasmacytoid DCs (pDCs), cycling T cells, basophils, T cells, and cycling AMs (Figure 5B), and the relative abundance of the populations recovered by scRNA-seq was also observed by flow analysis in the same tissue (Figures S5B and S5C).

Mapping the distribution of the AMs isolated from each of mAb-treated groups, we found distinct antibody-specific enrichment patterns across the subclustered AMs (Figure 5C), indicating that antibodies promoted shifts in AM transcriptional states. To identify distinct pathways induced in AMs of mAb-treated mice, we performed gene set enrichment analysis (GSEA) of the expressed genes measured within the pseudo-bulked AM subclusters in individual mice. We performed pairwise comparisons of cells from mIgG2a-, mIgG2a-N297A-, PBS control-treated, and infected mice. In AMs from restrictive mIgG2a antibody-treated mice, we consistently observed activation of DNA repair, heme metabolism, and reactive oxygen species (ROS) pathways (red dots) (Figure 5D). In the AMs from non-restrictive mIgG2a N297A-treated mice, we observed an enriched gene expression profile, which indicated an enhanced interferon-α (IFN-α) response accompanied by oxidative phosphorylation and Myc target gene activation (blue dots in mIgG2a/N297A comparisons and red dots in N297A/PBS comparisons) (Figure 5D). The GSEA of AMs revealed that transcriptional signature shifts, associated with the functional Fc variants, occurred prior to the onset of *M. tuberculosis* restriction in mice.

GSEA analysis on the pseudo-bulked neutrophils of the individually treated mice revealed additional Fc-mediated changes to lung neutrophil state. Several pathways were enriched within the cells from mIgG2a-treated mice versus mIgG2a N297A-treated or PBS control mice. No pathways reached significance in the comparison of N297A and PBS (Figure 5E). In the neutrophils of mIgG2a-treated mice, there was differential expression of fatty acid metabolism, G2M checkpoint, and Myc target genes (Figure 5E). Thus, single-cell sequencing revealed early shifts in cellular transcriptional circuitry ahead of observed *in vivo M. tuberculosis* control, coordinated by mAb-mediated cellular activation. Activation of these non-canonical pathways in AMs and PMNs may render cells of the lung more resistant to bacterial growth, resulting in acute *M. tuberculosis* restriction and delayed dissemination in mice.

DISCUSSION

Emerging data indicate that antibody function is a correlate of protection against TB.[16,43] *M. tuberculosis*-specific antibodies can enhance *M. tuberculosis* restriction *in vitro*, in macrophages[6,16,31] and human whole blood,[44] and *in vivo*, in mouse models of infection.[5,6,12] While antibodies able to opsonize *M. tuberculosis* are commonly associated with antimicrobial activity at early stages of *M. tuberculosis* infection *in vivo*,[6,7] the potential for antibodies targeting diverse *M. tuberculosis* antigens, including non-surface antigens, remains incompletely understood. By screening a library of mAbs targeting various *M. tuberculosis* intracellular, cell wall-associated, and secreted antigens, we found that antibody opsonization of *M. tuberculosis* and opsinophagocytic activity were concordant but did not correlate with *in vivo* restriction in mice. Instead, both opsonizing and non-opsonizing mAbs restricted *M. tuberculosis*, indicating that additional functions of antibodies may be responsible for antimicrobial activity *in vivo*. Further dissection of the *in vivo* immunological responses induced by

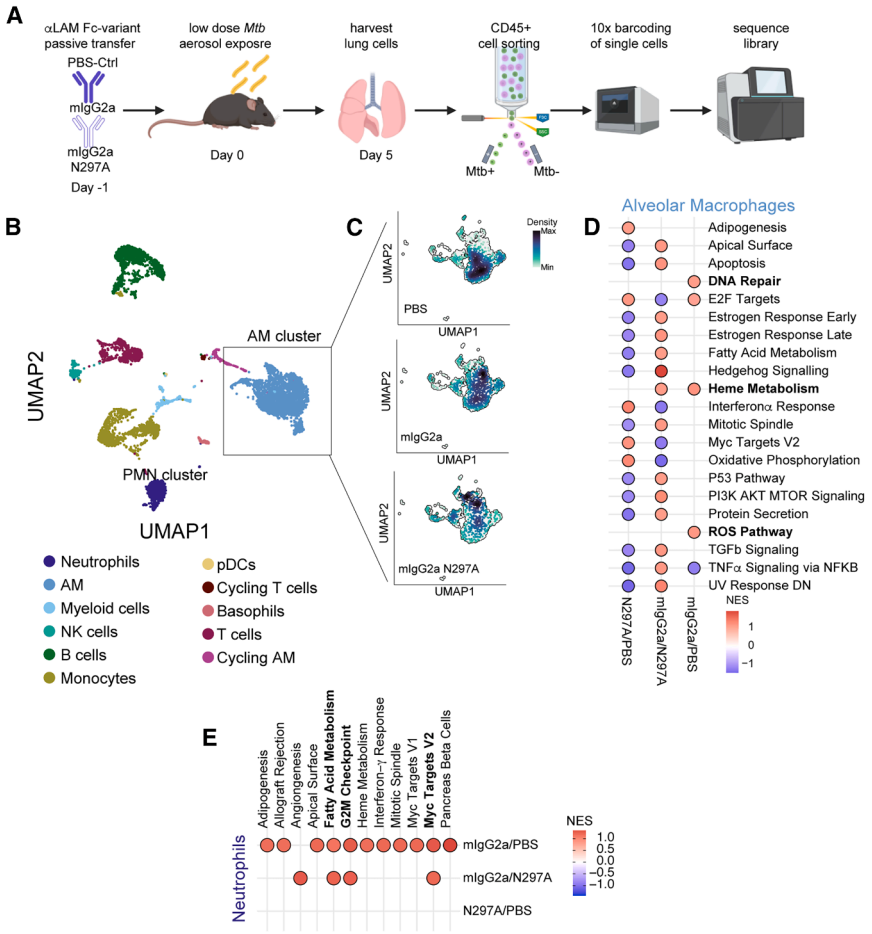

Figure 5. scRNA-seq of αLAM-mIgG2a-treated and –mIgG2a N297A-treated lung cells reveals distinct AM and PMN states

(A) C57BL/6 mice were pre-treated with 100 μg of αLAM (A194) and infected via aerosol with ~60 day 1 CFUs of YFP-*M. tuberculosis*.

(B) UMAP depicts clusters of immune cells defined from scRNA-seq: including neutrophils, alveolar macrophages (AMs), myeloid cells, NK cells, B cells, monocytes, plasmacytoid dendritic cells (pDCs), cycling T cells, basophils, T cells, and cycling AMs.

(C) Cells from the distinct Fc-variant treatment groups are differentially distributed within the AM subcluster.

(D) Top pathways of AM subcluster identified in gene set enrichment analysis (GSEA) in at least one of the following pairwise comparisons: mIgG2a/PBS, mIgG2a/N297A, N297A/PBS.

(E) Differentially enriched pathways within neutrophils identified in GSEA in at least one of the following pairwise comparisons: mIgG2a/PBS, mIgG2a/N297A, N297A/PBS. n = 3 mice per group. Enriched pathways depicted are derived from 100 permutations with normalized enrichment scores (NESs) > 1.1, signifying enrichment in the numerator (red dots), or NES < −1.3 signifying enrichment in the denominator (blue dots). Enriched pathways across the group comparisons with nominal p < 0.05 are filled with red for significant numerator enrichment or blue for denominator enrichment for the pairwise comparison.

See also Figure S5.

a LAM-specific mAb pointed to a clear Fc-dependent mechanism of protection, linked to an Fc-dependent shift of bacterial tropism across lung immune cells. In addition, we observed non-canonical transcriptional activation of immune cells early following *M. tuberculosis* infection. Together, these data point to a previously unappreciated role for antibodies in early *M. tuberculosis* restriction within the lung, if primed by a vaccine. In the setting of this LAM-specific mAb, the mAb alone did not clear the bacteria, but collaborates with cells responding to infection in the lung to promote bacterial clearance via transcriptional rewiring of key innate immune cell types.

We identified several mAbs capable of restricting *M. tuberculosis in vivo*, despite poor or negligible *M. tuberculosis* surface binding. These mAbs target counterintuitive antigens described as secreted or intracellular: Ag85B, Apa, Mpt64, and HspX. Consistent with our observations, antibodies against HspX and Ag85 were previously shown to protect against *M. tuberculosis* during passive transfer experiments in mice.[7,13] During infection, antigen targets have been identified in endocytic vesicles, which transport *M. tuberculosis* antigens to the extracellular space,[45] making these targets potentially accessible to antibodies independent of the bacterial surface. Antibody interactions with released antigens may form complexes that co-ligate FcRs on infected cells to promote eradication of intracellular *M. tuberculosis* or that engage FcRs to promote inflammatory responses.[46] In addition, Mpt64 has previously been identified in infected cell membranes[47]; antibodies specific for this and other cell surface-associated antigens could recruit cells to recognize and eliminate infected cells. In other infectious diseases, such as malaria and HIV, antibodies that bind the surface of infected cells can recruit FcR-bearing NK cells to induce antibody-dependent cellular cytotoxicity (ADCC) and enhance infection control.[48–50] Thus, antibodies targeting diversely localized *M. tuberculosis* antigens, such as those identified in our screen, may induce Fc-effector functions beyond bacterial phagocytosis and contribute to immune-mediated protection during *M. tuberculosis* infection.

Previous studies found an enrichment of antibodies with enhanced binding to FcγRIIIA in patients that controlled TB infection.[16] FcγRIIIA is an activating FcR that directs ADCC through NK cells and macrophages. Phenotypic analyses of peripheral blood mononuclear cells in a cohort of TB patients also identified increased expression of FcγRIIIA on NK cells in humans with controlled *M. tuberculosis* infection,[51] further implicating engagement of specific FcRs in TB control. Here, we demonstrate that αLAM Fc variants with the highest affinity for FcγRIV, the mouse FcR analog to human FcγRIIIA,[30,33] promoted robust restriction of *M. tuberculosis* infection *in vivo*. While mouse NK cells do not express FcγRIV, many myeloid cells, including AMs, express FcγRIV (Figure S6). As the first phagocytes to encounter *M. tuberculosis* during infection,

AMs may respond rapidly and robustly to antibody-opsonized *M. tuberculosis* and contribute to rapid bacterial capture or growth restriction.[37,52,53] Importantly, antibody-mediated FcγRIV ligation on AMs may play a critical role in antibody-mediated protection against influenza, as the depletion of AMs prior to viral challenge disrupted antibody-mediated restriction of influenza.[54] These data point to a critical role for early antibody-mediated activation of AMs as a first line of defense against *M. tuberculosis* and other respiratory pathogens, potentially linked to FcγRIV in mice or FcγRIIIA in humans.

Transcriptional profiling of the lung cellular immune response to mAb Fc-variant treatment following *M. tuberculosis* infection revealed distinct shifts in cell state following mAb variant treatment. We found early activation profiles associated with the restrictive αLAM mIgG2a, compared with controls in AMs and PMNs within the infected tissue. Consistent with previous studies of macrophages,[55] we found ROS signaling elevated in restrictive mIgG2a-treated lung AMs. In a model of lupus nephritis, antibody Fc has recently been found to shift liver macrophage metabolism following antibody treatment, and this metabolic shift promoted greater inflammatory responses to immune complexes.[56] Here, we found a heme metabolism pathway preferentially elevated in AMs in mice treated with the restrictive mIgG2a variant. Similarly, this pathway has been found to be enriched in *M. tuberculosis*-restrictive AMs in concomitantly immune animal models,[57] and transcriptional changes in BCG-trained immunity models also reveal heme metabolism enrichment.[58]

PMNs also displayed shifts in metabolism. Both fatty acid and heme metabolism gene sets were enriched in the lung PMNs of protective mIgG2a-treated mice, indicating that metabolic shifts in neutrophils may promote a less hospitable environment for bacterial growth. Although there is a paucity of data linking metabolism in PMNs to *M. tuberculosis* control,[59,60] recent studies have found that distinct metabolic activation of neutrophils can promote inflammation or prevent tissue damage.[61] While this study highlights a relationship of metabolism and antibody Fc recognition on immune cells, future studies are essential to understand how metabolic signals impact the cellular response during *M. tuberculosis* infection.

Recent TB vaccine studies point to a role for antibodies in *M. tuberculosis* control.[17] Likewise, intravenous BCG vaccination in non-human primates provides near sterilizing protection against *M. tuberculosis* and is linked to both cellular[62] and humoral immune responses.[18] Our current work contributes to the growing appreciation that humoral immunity contributes to protection against TB, extending our understanding of antigen targets and functional diversity of antibodies that promote bacterial control. Furthermore, the data presented here point to a critical collaboration between the humoral and innate immune response in early defense against *M. tuberculosis*. Thus, next-generation TB vaccines that exploit canonical (opsinophagocytosis and ADCC) and non-canonical (metabolic) functions may enhance clearance of this deadly pathogen.

This study raises hypotheses for future investigation. The antigen targets of the protective Fab identified in our screen could be targeted by antibodies in novel vaccines to protect against TB, as has been achieved by antibodies in other bacteria-targeting vaccines.[63,64] Future studies, aimed at driving persistent and high titers of polyclonal antibodies to these antigens, would provide additional insights into the mechanisms by which *M. tuberculosis* surface- and non-surface-associated antibodies promote bacterial restriction *in vivo*. Our findings also indicate that high concentrations of non-specific isotype IgG2a can induce antimicrobial activity in the lungs of *M. tuberculosis*-infected mice, indicating a response to monomeric antibody Fc engagement of FcRs.[65,66] Importantly, we find that only the combination of antigen-specific targeting and Fc function promotes significant changes in *M. tuberculosis* tropism and immune cell state.

Limitations of the study

Here, we focused on the role of antibodies as a prophylactic measure against *M. tuberculosis* infection. In our model, antibodies engage innate immune cells in the absence of T cells. However, in vaccination or therapy, antibodies would be persistent, tonically interacting with circulating *M. tuberculosis* antigen and the innate immune system and likely collaborating with T cells. Several *M. tuberculosis* infection models indicate that antibody-mediated function can be dependent on T cells,[3,5] and future studies will be essential to fully dissect the precise antibody Fc biology that best cooperates with T cell immunity to gain optimal control over *M. tuberculosis* infection.

RESOURCE AVAILABILITY

Lead contact

Further information and requests for resources and reagents should be directed to and will be fulfilled by the lead contact, Galit Alter (galter@partners.org).

Materials availability

mAbs generated in this study are available on request.

Data and code availability

In addition to data included within the main text and supplemental information, flow cytometry and meta data associated with mouse immune profiling can be found online (https://fairdomhub.org/studies/927) along with the tabulated immune cell measures derived from flow files and gates. scRNA-seq files are deposited in GEO and analysis code on (Zenodo). Accession numbers are listed in the key resources table. All data are publicly available from the date of publication. Any additional information required to reanalyze the data reported in this paper is available from the lead contact upon request.

ACKNOWLEDGMENTS

We thank Karen Dobos, Hui-Chen Chang Foreman, and Timothy Stedman for sharing antibody sequences of clones in the BEI Resources repository.[29] We thank the Dana Farber Cancer Institute for large-scale mAb production, Duke Human Vaccine Institute for providing us with the avi-tagged mouse FcR reagents, and the Ragon Institute Flow Cytometry for expertise and technical assistance with sample analysis and sorting. Finally, we are grateful to the BioMIcro Center, Data Management and Analysis Core of MIT for data management support. The authors acknowledge funding by the Ragon Institute of MGH, MIT, and Harvard and the SAMANA Kay MGH Research Scholar Program (G.A.); the Bill and Melinda Gates Foundation grant OPP1156795 (G.A. and S.M.F.); the National Institutes of Health definitive contract no.75N93019C00071 (S.M.F., G.A., B.D.B., and C.M.S.); the National Institutes of Health grant T32 AI007061 (P.S.G.); and the Yerby Fellowship Program (P.S.G.).

AUTHOR CONTRIBUTIONS

Conceptualization, P.S.G., G.A., and S.M.F.; methodology, P.S.G., J.M.P., J. S., R.L., B.A.F., A.V., M.D.S., E.B.I., M.K.P., C.M.S., A. Casadevall, A. Choudhary, A.P., R.R., C. Locht, G.K., R.D.C., M.-H.W., T.M., B.D.B., G.A., and S.M.F.; investigation, P.S.G., G.A., and S.M.F.; visualization, P.S.G. and J.M.P.; funding acquisition, G.A. and S.M.F.; project administration, C. Luedeman; supervision, G.A. and S.M.F.; writing – original draft, P.S.G., G.A., and S.M.F.; writing – review & editing, all authors.

DECLARATION OF INTERESTS

G.A. is a founder of SeromYx Systems.

STAR★METHODS

Detailed methods are provided in the online version of this paper and include the following:

- KEY RESOURCES TABLE
- EXPERIMENTAL MODEL AND STUDY PARTICIPANT DETAILS
  - Mice
  - Bone marrow derived dendritic cells, macrophages, and neutrophils
  - Bacterial Strains
- METHOD DETAILS
  - Aerosol infection of mice
  - Antibody cloning and expression
  - Mtb surface staining
  - LAM coated bead phagocytic assays
  - Mtb Phagocytic Assays in bone marrow derived cells
  - IC50 determination for LAM mAbs
  - Luminex-based FcR-binding assay
  - Luminex-based complement deposition assay
  - Flow staining of infected lungs
  - Mtb restriction assay in sorted lung immune cells
  - Single-cell sorting and RNA Sequencing of mouse lung cells
  - Analysis of infection scRNA-seq data
  - Gene Set Enrichment Analysis
  - Data Analysis and Visualization
- QUANTIFICATION AND STATISTICAL ANALYSIS

SUPPLEMENTAL INFORMATION

Supplemental information can be found online at https://doi.org/10.1016/j.immuni.2025.05.004.

Received: October 20, 2024
Revised: January 31, 2025
Accepted: May 7, 2025
Published: June 10, 2025

REFERENCES

1. World Health Organization. (2020). Global Tuberculosis Report 2020. https://www.who.int/publications/i/item/9789240013131.,
2. Mayer-Barber, K.D., and Barber, D.L. (2015). Innate and Adaptive Cellular Immune Responses to Mycobacterium tuberculosis Infection. Cold Spring Harb. Perspect. Med. *5*, a018424. https://doi.org/10.1101/cshperspect.a018424.
3. Roy, E., Stavropoulos, E., Brennan, J., Coade, S., Grigorieva, E., Walker, B., Dagg, B., Tascon, R.E., Lowrie, D.B., Colston, M.J., et al. (2005). Therapeutic efficacy of high-dose intravenous immunoglobulin in Mycobacterium tuberculosis infection in mice. Infect. Immun. *73*, 6101–6109. https://doi.org/10.1128/IAI.73.9.6101-6109.2005.
4. Olivares, N., Puig, A., Aguilar, D., Moya, A., Cádiz, A., Otero, O., Izquierdo, L., Falero, G., Solis, R.L., Orozco, H., et al. (2009). Prophylactic effect of administration of human gamma globulins in a mouse model of tuberculosis. Tuberc. Edinb. Scotl. *89*, 218–220. https://doi.org/10.1016/j.tube.2009.02.003.
5. Li, H., Wang, X.-X., Wang, B., Fu, L., Liu, G., Lu, Y., Cao, M., Huang, H., and Javid, B. (2017). Latently and uninfected healthcare workers exposed to TB make protective antibodies against Mycobacterium tuberculosis. Proc. Natl. Acad. Sci. USA *114*, 5023–5028. https://doi.org/10.1073/pnas.1611776114.
6. Chen, T., Blanc, C., Liu, Y., Ishida, E., Singer, S., Xu, J., Joe, M., Jenny-Avital, E.R., Chan, J., Lowary, T.L., et al. (2020). Capsular glycan recognition provides antibody-mediated immunity against tuberculosis. J. Clin. Invest. *130*, 1808–1822. https://doi.org/10.1172/JCI128459.
7. Prados-Rosales, R., Carre, o.L., Cheng, T., Blanc, C., Weinrick, B., Malek, A., Lowary, T.L., Baena, A., Joe, M., et al. (2017). Enhanced control of Mycobacterium tuberculosis extrapulmonary dissemination in mice by an arabinomannan-protein conjugate vaccine. PLoS Pathog. *13*, e1006250. https://doi.org/10.1371/journal.ppat.1006250.
8. Lyashchenko, K., Colangeli, R., Houde, M., Al Jahdali, H.A., Menzies, D., and Gennaro, M.L. (1998). Heterogeneous Antibody Responses in Tuberculosis. Infect. Immun. *66*, 3936–3940. https://doi.org/10.1128/IAI.66.8.3936-3940.1998.
9. Hamasur, B., Haile, M., Pawlowski, A., Schroder, U., Kallenius, G., and Svenson, S.B. (2004). A mycobacterial lipoarabinomannan specific monoclonal antibody and its F(ab′) fragment prolong survival of mice infected with Mycobacterium tuberculosis. Clin. Exp. Immunol. *138*, 30–38. https://doi.org/10.1111/j.1365-2249.2004.02593.x.
10. Teitelbaum, R., Glatman-Freedman, A., Chen, B., Robbins, J.B., Unanue, E., Casadevall, A., and Bloom, B.R. (1998). A mAb recognizing a surface antigen of Mycobacterium tuberculosis enhances host survival. Proc. Natl. Acad. Sci. USA *95*, 15688–15693. https://doi.org/10.1073/pnas.95.26.15688.
11. Pethe, K., Alonso, S., Biet, F., Delogu, G., Brennan, M.J., Locht, C., and Menozzi, F.D. (2001). The heparin-binding haemagglutinin of M. tuberculosis is required for extrapulmonary dissemination. Nature *412*, 190–194. https://doi.org/10.1038/35084083.
12. Watson, A., Li, H., Ma, B., Weiss, R., Bendayan, D., Abramovitz, L., Ben-Shalom, N., Mor, M., Pinko, E., Bar Oz, M.B., et al. (2021). Human antibodies targeting a Mycobacterium transporter protein mediate protection against tuberculosis. Nat. Commun. *12*, 602. https://doi.org/10.1038/s41467-021-20930-0.
13. Balu, S., Reljic, R., Lewis, M.J., Pleass, R.J., McIntosh, R., van Kooten, C., van Egmond, M., Challacombe, S., Woof, J.M., and Ivanyi, J. (2011). A novel human IgA monoclonal antibody protects against tuberculosis. J. Immunol. *186*, 3113–3119. https://doi.org/10.4049/jimmunol.1003189.
14. Bournazos, S., DiLillo, D.J., and Ravetch, J.V. (2015). The role of Fc–FcγR interactions in IgG-mediated microbial neutralization. J. Exp. Med. *212*, 1361–1369. https://doi.org/10.1084/jem.20151267.
15. Lu, L.L., Suscovich, T.J., Fortune, S.M., and Alter, G. (2018). Beyond binding: antibody effector functions in infectious diseases. Nat. Rev. Immunol. *18*, 46–61. https://doi.org/10.1038/nri.2017.106.
16. Lu, L.L., Chung, A.W., Rosebrock, T.R., Ghebremichael, M., Yu, W.H., Grace, P.S., Schoen, M.K., Tafesse, F., Martin, C., Leung, V., et al. (2016). A Functional Role for Antibodies in Tuberculosis. Cell *167*, 433–443.e14. https://doi.org/10.1016/j.cell.2016.08.072.
17. Fletcher, H.A., Snowden, M.A., Landry, B., Rida, W., Satti, I., Harris, S.A., Matsumiya, M., Tanner, R., O'Shea, M.K., Dheenadhayalan, V., et al. (2016). T-cell activation is an immune correlate of risk in BCG vaccinated infants. Nat. Commun. *7*, 11290. https://doi.org/10.1038/ncomms11290.
18. Irvine, E.B., O'Neil, A., Darrah, P.A., Shin, S., Choudhary, A., Li, W., Honnen, W., Mehra, S., Kaushal, D., Gideon, H.P., et al. (2021). Robust IgM responses following intravenous vaccination with Bacille Calmette–Guérin associate with prevention of Mycobacterium tuberculosis infection in macaques. Nat. Immunol. *22*, 1515–1523. https://doi.org/10.1038/s41590-021-01066-1.
19. Maglione, P.J., Xu, J., Casadevall, A., and Chan, J. (2008). Fc gamma receptors regulate immune activation and susceptibility during

Mycobacterium tuberculosis infection. J. Immunol. *180*, 3329–3338. https://doi.org/10.4049/jimmunol.180.5.3329.

20. Liu, Y., Chen, T., Zhu, Y., Furey, A., Lowary, T.L., Chan, J., Bournazos, S., Ravetch, J.V., and Achkar, J.M. (2023). Features and protective efficacy of human mAbs targeting Mycobacterium tuberculosis arabinomannan. JCI Insight *8*, e167960. https://doi.org/10.1172/jci.insight.167960.
21. Zimmermann, N., Thormann, V., Hu, B., Köhler, A.B., Imai-Matsushima, A., Locht, C., Arnett, E., Schlesinger, L.S., Zoller, T., Schürmann, M., et al. (2016). Human isotype-dependent inhibitory antibody responses against Mycobacterium tuberculosis. EMBO Mol. Med. *8*, 1325–1339. https://doi.org/10.15252/emmm.201606330.
22. Hermann, C., and King, C.G. (2021). TB or not to be: what specificities and impact do antibodies have during tuberculosis? Oxf. Open Immunol. *2*, iqab015. https://doi.org/10.1093/oxfimm/iqab015.
23. Fujita, Y., Doi, T., Sato, K., and Yano, I. (2005). Diverse humoral immune responses and changes in IgG antibody levels against mycobacterial lipid antigens in active tuberculosis. Microbiology (Reading) *151*, 2065–2074. https://doi.org/10.1099/mic.0.27790-0.
24. Glatman-Freedman, A., and Casadevall, A. (1998). Serum Therapy for Tuberculosis Revisited: Reappraisal of the Role of Antibody-Mediated Immunity against Mycobacterium tuberculosis. Clin. Microbiol. Rev. *11*, 514–532. https://doi.org/10.1128/CMR.11.3.514.
25. Ishida, E., Corrigan, D.T., Malonis, R.J., Hofmann, D., Chen, T., Amin, A.G., Chatterjee, D., Joe, M., Lowary, T.L., Lai, J.R., et al. (2021). Monoclonal antibodies from humans with Mycobacterium tuberculosis exposure or latent infection recognize distinct arabinomannan epitopes. Commun. Biol. *4*, 1181. https://doi.org/10.1038/s42003-021-02714-w.
26. Chatterjee, D., Lowell, K., Rivoire, B., McNeil, M.R., and Brennan, P.J. (1992). Lipoarabinomannan of Mycobacterium tuberculosis. Capping with mannosyl residues in some strains. J. Biol. Chem. *267*, 6234–6239. https://doi.org/10.1016/s0021-9258(18)42686-5.
27. Ernst, J.D., Cornelius, A., and Bolz, M. (2019). Dynamics of Mycobacterium tuberculosis Ag85B Revealed by a Sensitive Enzyme-Linked Immunosorbent Assay. mBio *10*, e00611-19. https://doi.org/10.1128/mBio.00611-19.
28. Choudhary, A., Patel, D., Honnen, W., Lai, Z., Prattipati, R.S., Zheng, R.B., Hsueh, Y.-C., Gennaro, M.L., Lardizabal, A., Restrepo, B.I., et al. (2018). Characterization of the Antigenic Heterogeneity of Lipoarabinomannan, the Major Surface Glycolipid of Mycobacterium tuberculosis, and Complexity of Antibody Specificities toward This Antigen. J. Immunol. *200*, 3053–3066. https://doi.org/10.4049/jimmunol.1701673.
29. Foreman, H.C.C., Frank, A., and Stedman, T.T. (2021). Determination of variable region sequences from hybridoma immunoglobulins that target Mycobacterium tuberculosis virulence factors. PLoS One *16*, e0256079. https://doi.org/10.1371/journal.pone.0256079.
30. Overdijk, M.B., Verploegen, S., Ortiz Buijsse, A., Vink, T., Leusen, J.H.W., Bleeker, W.K., and Parren, P.W.H.I. (2012). Crosstalk between human IgG isotypes and murine effector cells. J. Immunol. *189*, 3430–3438. https://doi.org/10.4049/jimmunol.1200356.
31. Chen, T., Blanc, C., Eder, A.Z., Prados-Rosales, R., Souza, A.C.O., Kim, R. S., Glatman-Freedman, A., Joe, M., Bai, Y., Lowary, T.L., et al. (2016). Association of Human Antibodies to Arabinomannan With Enhanced Mycobacterial Opsonophagocytosis and Intracellular Growth Reduction. J. Infect. Dis. *214*, 300–310. https://doi.org/10.1093/infdis/jiw141.
32. Joller, N., Weber, S.S., Müller, A.J., Spörri, R., Selchow, P., Sander, P., Hilbi, H., and Oxenius, A. (2010). Antibodies protect against intracellular bacteria by Fc receptor-mediated lysosomal targeting. Proc. Natl. Acad. Sci. USA *107*, 20441–20446. https://doi.org/10.1073/pnas.1013827107.
33. Nimmerjahn, F., Bruhns, P., Horiuchi, K., and Ravetch, J.V. (2005). FcγRIV: A Novel FcR with Distinct IgG Subclass Specificity. Immunity *23*, 41–51. https://doi.org/10.1016/j.immuni.2005.05.010.
34. Biburger, M., Aschermann, S., Schwab, I., Lux, A., Albert, H., Danzer, H., Woigk, M., Dudziak, D., and Nimmerjahn, F. (2011). Monocyte Subsets Responsible for Immunoglobulin G-Dependent Effector Functions In Vivo. Immunity *35*, 932–944. https://doi.org/10.1016/j.immuni.2011.11.009.
35. Yu, Y.-R.A., O'Koren, E.G., Hotten, D.F., Kan, M.J., Kopin, D., Nelson, E. R., Que, L., and Gunn, M.D. (2016). A Protocol for the Comprehensive Flow Cytometric Analysis of Immune Cells in Normal and Inflamed Murine Non-Lymphoid Tissues. PLoS One *11*, e0150606. https://doi.org/10.1371/journal.pone.0150606.
36. Misharin, A.V., Morales-Nebreda, L., Mutlu, G.M., Budinger, G.R.S., and Perlman, H. (2013). Flow Cytometric Analysis of Macrophages and Dendritic Cell Subsets in the Mouse Lung. Am. J. Respir. Cell Mol. Biol. *49*, 503–510. https://doi.org/10.1165/rcmb.2013-0086MA.
37. Cohen, S.B., Gern, B.H., Delahaye, J.L., Adams, K.N., Plumlee, C.R., Winkler, J.K., Sherman, D.R., Gerner, M.Y., and Urdahl, K.B. (2018). Alveolar Macrophages Provide an Early Mycobacterium tuberculosis Niche and Initiate Dissemination. Cell Host Microbe *24*, 439–446.e4. https://doi.org/10.1016/j.chom.2018.08.001.
38. Wolf, A.J., Linas, B., Trevejo-Nuñez, G.J., Kincaid, E., Tamura, T., Takatsu, K., and Ernst, J.D. (2007). Mycobacterium tuberculosis infects dendritic cells with high frequency and impairs their function in vivo. J. Immunol. *179*, 2509–2519. https://doi.org/10.4049/jimmunol.179.4.2509.
39. Wolf, A.J., Desvignes, L., Linas, B., Banaiee, N., Tamura, T., Takatsu, K., and Ernst, J.D. (2008). Initiation of the adaptive immune response to Mycobacterium tuberculosis depends on antigen production in the local lymph node, not the lungs. J. Exp. Med. *205*, 105–115. https://doi.org/10.1084/jem.20071367.
40. Vieira, P., and Rajewsky, K. (1988). The half-lives of serum immunoglobulins in adult mice. Eur. J. Immunol. *18*, 313–316. https://doi.org/10.1002/eji.1830180221.
41. Petkova, S.B., Akilesh, S., Sproule, T.J., Christianson, G.J., Al Khabbaz, H., Brown, A.C., Presta, L.G., Meng, Y.G., and Roopenian, D.C. (2006). Enhanced half-life of genetically engineered human IgG1 antibodies in a humanized FcRn mouse model: potential application in humorally mediated autoimmune disease. Int. Immunol. *18*, 1759–1769. https://doi.org/10.1093/intimm/dxl110.
42. Tabula; Muris Consortium; Overall coordination; Logistical coordination; Organ collection and processing; Library preparation and sequencing; Computational data analysis; Cell type annotation; Writing group; Supplemental text writing group; Principal investigators (2018). Single-cell transcriptomics of 20 mouse organs creates a Tabula Muris. Nature *562*, 367–372. https://doi.org/10.1038/s41586-018-0590-4.
43. Lu, L.L., Smith, M.T., Yu, K.K.Q., Luedemann, C., Suscovich, T.J., Grace, P.S., Cain, A., Yu, W.H., McKitrick, T.R., Lauffenburger, D., et al. (2019). IFN-γ-independent immune markers of Mycobacterium tuberculosis exposure. Nat. Med. *25*, 977–987. https://doi.org/10.1038/s41591-019-0441-3.
44. Irvine, E.B., Peters, J.M., Lu, R., Grace, P.S., Sixsmith, J., Wallace, A., Schneider, M., Shin, S., Karpinski, W., Hsiao, J.C., et al. (2022). Fc-engineered antibodies leverage neutrophils to drive control of Mycobacterium tuberculosis. Nat. Microbiol. *9*, 2369–2382. https://doi.org/10.1101/2022.05.01.490220.
45. Wang, J., Wang, Y., Tang, L., and Garcia, R.C. (2019). Extracellular Vesicles in Mycobacterial Infections: Their Potential as Molecule Transfer Vectors. Front. Immunol. *10*, 1929. https://doi.org/10.3389/fimmu.2019.01929.
46. Clynes, R., Maizes, J.S., Guinamard, R., Ono, M., Takai, T., and Ravetch, J.V. (1999). Modulation of Immune Complex–induced Inflammation In Vivo by the Coordinate Expression of Activation and Inhibitory Fc Receptors. J. Exp. Med. *189*, 179–185. https://doi.org/10.1084/jem.189.1.179.
47. Stamm, C.E., Pasko, B.L., Chaisavaneeyakorn, S., Franco, L.H., Nair, V. R., Weigele, B.A., Alto, N.M., and Shiloh, M.U. (2019). Screening Mycobacterium tuberculosis Secreted Proteins Identifies Mpt64 as a Eukaryotic Membrane-Binding Bacterial Effector. mSphere *4*, e00354-19. https://doi.org/10.1128/mSphere.00354-19.
48. Chung, A.W., Kumar, M.P., Arnold, K.B., Yu, W.H., Schoen, M.K., Dunphy, L.J., Suscovich, T.J., Frahm, N., Linde, C., Mahan, A.E., et al. (2015).

Dissecting Polyclonal Vaccine-Induced Humoral Immunity against HIV Using Systems Serology. Cell *163*, 988–998. https://doi.org/10.1016/j.cell.2015.10.027.

49. Arora, G., Hart, G.T., Manzella-Lapeira, J., Doritchamou, J.Y.A., Narum, D. L., Thomas, L.M., Brzostowski, J., Rajagopalan, S., Doumbo, O.K., Traore, B., et al. (2018). NK cells inhibit Plasmodium falciparum growth in red blood cells via antibody-dependent cellular cytotoxicity. eLife *7*, e36806. https://doi.org/10.7554/eLife.36806.
50. Clayton, K.L., Mylvaganam, G., Villasmil-Ocando, A., Stuart, H., Maus, M. V., Rashidian, M., Ploegh, H.L., and Walker, B.D. (2021). HIV-infected macrophages resist efficient NK cell-mediated killing while preserving inflammatory cytokine responses. Cell Host Microbe *29*, 435–447.e9. https://doi.org/10.1016/j.chom.2021.01.006.
51. Chowdhury, R.R., Vallania, F., Yang, Q., Angel, C.J.L., Darboe, F., Penn-Nicholson, A., Rozot, V., Nemes, E., Malherbe, S.T., Ronacher, K., et al. (2018). A multi-cohort study of the immune factors associated with M. tuberculosis infection outcomes. Nature *560*, 644–648. https://doi.org/10.1038/s41586-018-0439-x.
52. Huang, L., Nazarova, E.V., Tan, S., Liu, Y., and Russell, D.G. (2018). Growth of Mycobacterium tuberculosis in vivo segregates with host macrophage metabolism and ontogeny. J. Exp. Med. *215*, 1135–1152. https://doi.org/10.1084/jem.20172020.
53. Rothchild, A.C., Olson, G.S., Nemeth, J., Amon, L.M., Mai, D., Gold, E.S., Diercks, A.H., and Aderem, A. (2019). Alveolar macrophages generate a noncanonical NRF2-driven transcriptional response to Mycobacterium tuberculosis in vivo. Sci. Immunol. *4*, eaaw6693. https://doi.org/10.1126/sciimmunol.aaw6693.
54. He, W., Chen, C.-J., Mullarkey, C.E., Hamilton, J.R., Wong, C.K., Leon, P. E., Uccellini, M.B., Chromikova, V., Henry, C., Hoffman, K.W., et al. (2017). Alveolar macrophages are critical for broadly-reactive antibody-mediated protection against influenza A virus in mice. Nat. Commun. *8*, 846. https://doi.org/10.1038/s41467-017-00928-3.
55. Zimmerer, J.M., Liu, X.L., Blaszczak, A., Avila, C.L., Pham, T.A., Warren, R. T., and Bumgardner, G.L. (2018). Critical Role of Macrophage FcγR Signaling and Reactive Oxygen Species in Alloantibody-Mediated Hepatocyte Rejection. J. Immunol. *201*, 3731–3740. https://doi.org/10.4049/jimmunol.1800333.
56. Jing, C., Castro-Dopico, T., Richoz, N., Tuong, Z.K., Ferdinand, J.R., Lok, L.S.C., Loudon, K.W., Banham, G.D., Mathews, R.J., Cader, Z., et al. (2020). Macrophage metabolic reprogramming presents a therapeutic target in lupus nephritis. Proc. Natl. Acad. Sci. USA *117*, 15160–15171. https://doi.org/10.1073/pnas.2000943117.
57. Nemeth, J., Olson, G.S., Rothchild, A.C., Jahn, A.N., Mai, D., Duffy, F.J., Delahaye, J.L., Srivatsan, S., Plumlee, C.R., Urdahl, K.B., et al. (2020). Contained Mycobacterium tuberculosis infection induces concomitant and heterologous protection. PLoS Pathog. *16*, e1008655. https://doi.org/10.1371/journal.ppat.1008655.
58. Khan, N., Downey, J., Sanz, J., Kaufmann, E., Blankenhaus, B., Pacis, A., Pernet, E., Ahmed, E., Cardoso, S., Nijnik, A., et al. (2020). M. tuberculosis Reprograms Hematopoietic Stem Cells to Limit Myelopoiesis and Impair Trained Immunity. Cell *183*, 752–770.e22. https://doi.org/10.1016/j.cell.2020.09.062.
59. Pisu, D., Huang, L., Grenier, J.K., and Russell, D.G. (2020). Dual RNA-Seq of Mtb-Infected Macrophages In Vivo Reveals Ontologically Distinct Host-Pathogen Interactions. Cell Rep. *30*, 335–350.e4. https://doi.org/10.1016/j.celrep.2019.12.033.
60. Pisu, D., Huang, L., Narang, V., Theriault, M., Lê-Bury, G., Lee, B., Lakudzala, A.E., Mzinza, D.T., Mhango, D.V., Mitini-Nkhoma, S.C., et al. (2021). Single cell analysis of M. tuberculosis phenotype and macrophage lineages in the infected lung. J. Exp. Med. *218*, e20210615. https://doi.org/10.1084/jem.20210615.
61. Morrison, T., Watts, E.R., Sadiku, P., and Walmsley, S.R. (2023). The emerging role for metabolism in fueling neutrophilic inflammation. Immunol. Rev. *314*, 427–441. https://doi.org/10.1111/imr.13157.
62. Darrah, P.A., Zeppa, J.J., Maiello, P., Hackney, J.A., Wadsworth, M.H., Hughes, T.K., Pokkali, S., Swanson, P.A., Grant, N.L., Rodgers, M.A., et al. (2020). Prevention of tuberculosis in macaques after intravenous BCG immunization. Nature *577*, 95–102. https://doi.org/10.1038/s41586-019-1817-8.
63. Andrews, N., Borrow, R., and Miller, E. (2003). Validation of Serological Correlate of Protection for Meningococcal C Conjugate Vaccine by Using Efficacy Estimates from Postlicensure Surveillance in England. Clin. Diagn. Lab. Immunol. *10*, 780–786. https://doi.org/10.1128/cdli.10.5.780-786.2003.
64. Westerink, M.A.J., Schroeder, H.W., and Nahm, M.H. (2012). Immune Responses to pneumococcal vaccines in children and adults: Rationale for age-specific vaccination. Aging Dis. *3*, 51–67.
65. Hulett, M.D., and Hogarth, P.M. (1998). The second and third extracellular domains of FcγRI (CD64) confer the unique high affinity binding of IgG2a. Mol. Immunol. *35*, 989–996. https://doi.org/10.1016/s0161-5890(98)00069-8.
66. Barnes, N., Gavin, A.L., Tan, P.S., Mottram, P., Koentgen, F., and Hogarth, P.M. (2002). FcγRI-Deficient Mice Show Multiple Alterations to Inflammatory and Immune Responses. Immunity *16*, 379–389. https://doi.org/10.1016/s1074-7613(02)00287-x.
67. Hao, Y., Hao, S., Andersen-Nissen, E., Mauck, W.M., Zheng, S., Butler, A., Lee, M.J., Wilk, A.J., Darby, C., Zager, M., et al. (2021). Integrated analysis of multimodal single-cell data. Cell *184*, 3573–3587.e29. https://doi.org/10.1016/j.cell.2021.04.048.
68. Schwebach, J.R., Glatman-Freedman, A., Gunther-Cummins, L., Dai, Z., Robbins, J.B., Schneerson, R., and Casadevall, A. (2002). Glucan Is a Component of the Mycobacterium tuberculosis Surface That Is Expressed In Vitro and In Vivo. Infect. Immun. *70*, 2566–2575. https://doi.org/10.1128/IAI.70.5.2566-2575.2002.
69. Atyeo, C., Slein, M.D., Fischinger, S., Burke, J., Schäfer, A., Leist, S.R., Kuzmina, N.A., Mire, C., Honko, A., Johnson, R., et al. (2021). Dissecting strategies to tune the therapeutic potential of SARS-CoV-2–specific monoclonal antibody CR3022. JCI Insight *6*, e143129. https://doi.org/10.1172/jci.insight.143129.
70. Liberzon, A., Birger, C., Thorvaldsdóttir, H., Ghandi, M., Mesirov, J.P., and Tamayo, P. (2015). The Molecular Signatures Database (MSigDB) Hallmark Gene Set Collection. Cell Syst. *1*, 417–425. https://doi.org/10.1016/j.cels.2015.12.004.

STAR★METHODS

KEY RESOURCES TABLE

REAGENT or RESOURCE	SOURCE	IDENTIFIER
Antibodies		
InVivoMAb human IgG1 isotype control	BioXCell	Cat # BE0297
InVivoMAb mouse IGg2a isotype control (clone C1.18.4)	BioXCell	Cat # BE0085
anti-CD45 (clone 30-F11) BUV395	BD	Cat # 564279
anti-CD11c (clone N418) PerCP	Biolegend	Cat # 117326
anti-Ly6G (clone 1A8) BV605	Biolegend	Cat # 127639
anti-Ly6C (clone HK1.4) AlexaFluor700	Biolegend	Cat # 128024
anti-IAIE (clone M5/114.15.2) BV421	BD	Cat # 562564
anti-CD24 (clone M1/69) BV510	Biolegend	Cat # 101806
anti-CD103 (clone 2E7) APC	Biolegend	Cat # 121413
anti-CD64 (clone X54-5/7.1 FC) PE-Cy7	Biolegend	Cat # 139314
anti-CD16/CD32 (clone 93) BV711	Biolegend	Cat # 101337
anti-CD16.2 (clone 9e9) BV785	Biolegend	Cat # 149535
anti-CD19 (clone 1D3) BUV737	BD	Cat # 612781
anti-CD11b (clone M1/70) BUV805	BD	Cat # 741934
anti-Siglec F (clone E50-2440) PE-CF594	BD	Cat # 562757
anti-cd351, Fca/mR (clone TX61) PE	Biolegend	Cat # 137306
Anti-human IgG1 Fc (clone M1310G05) APC	Biolegend	Cat # 410712
Anti-human IgG-Fc Fragment (polyclonal) HRP	Bethyl Laboratory	Cat # A80-104P
Anti-guinea pig complement C3 (polyclonal goat IgG) FITC	MP Biomedicals	Cat # 0855385
Bacterial and virus strains		
M. tuberculosis: YFP-tagged H37Rv	Laboratory of Chris Sasseti	N/A
M. tuberculosis: H37Rv	ATCC	ATCC 27294
M. tuberculosis: Lux276-H37Rv	Laboratory of Bryan Bryson	N/A
Chemicals, peptides, and recombinant proteins		
eBioscience™ Fixable Viability Dye eFluor™, 455UV	Thermo Fisher	Cat # 65-0868-18
LIVE/DEAD™ Fixable Near-IR Dead Cell Stain Kit	Thermo Fisher	Cat # L34975
LIVE/DEAD™ Fixable Yellow Dead Cell Stain Kit	Thermo Fisher	Cat # L34967
Recombinant Mouse FcgRIV, avi-tagged	Duke Human Vaccine Institute	N/A
Recombinant Mouse FcgRIII, avi-tagged	Duke Human Vaccine Institute	N/A
Recombinant Mouse FcgRIIB, avi-tagged	Duke Human Vaccine Institute	N/A
Streptavidin-PE	Prozyme	Cat # PJ31S
Lipoarabinomannan (LAM)	BEI Resources	Cat # NR-14848
HspX, Recombinant Protein Reference Standard Mycobacterium tuberculosis	BEI Resources	Cat # NR-49428
PstS1 (Gene Rv0934, Non-Acylated), Purified Native Protein from Strain, H37Rv Mycobacterium tuberculosis	BEI Resources	Cat # NR-14859
ESAT-6, Recombinant Protein Reference Standard Mycobacterium tuberculosis	BEI Resources	Cat # NR-49424
CFP-10, Recombinant Protein Reference Standard Mycobacterium tuberculosis	BEI Resources	Cat # NR-49425
Mouse GM-CSF, recombinant protein	PeproTech	Cat # 315-03-20UG
Mouse M-CSF, recombinant protein	PeproTech	Cat # 315-02-10UG
Middlebrook 7H9 Broth Base	Millipore Sigma	Cat # M0178-500G

(*Continued on next page*)

Continued

REAGENT or RESOURCE	SOURCE	IDENTIFIER
Middlebrook 7H11 Agar Base	Millipore SIgma	Cat # M0428-500G
Middlebrook OADC Growth Supplement	Millipore Sigma	Cat # M0678-500ML
Critical commercial assays		
Gelatin Veronal Buffer with Mg & Ca (GVB++)	Millipore Sigma	Cat # G6514
Low-Tox Guinea Pig Complement	Cedar Lane Labs	Cat # CL4051
Collagenase, Type 4, Filtered	Worthington	CLSS-4/LS004210
DNase I	Millipore Sigma	#10104159001
gentleMACS C Tubes	Miltenyi	Cat # 130-096-334
anti-mouse CD11c MicroBeads	Miltenyi	Cat # 130-125-835
anti-Ly6G MicroBeads	Miltenyi	Cat # 130-120-337
LS Columns	Miltenyi	Cat # 130-042-201
Chromium Single Cell 3' Reagent Kits (v3.1 Chemistry)	10X Genomics	Cat # PN-1000121
MULTI-seq Lipid-Modified Oligos	Millipore Sigma	Cat # LMO001
BD OptEIA™ TMB Substrate Reagent Set	BD	Cat # 555214
MagPlex microspheres	Diasorin	Cat # MC10045-YY, MC10009-YY, MC12024-01, MC10056-YY, MC10038-YY
FluoSpheres® NeutrAvidin®-Labeled Microspheres, 1.0 μm, yellow-green	Thermo Fisher	Cat #: F8776
Deposited data		
Raw data scRNAseq (Figure 5)	This paper	GEO: GSE198064
Flow cytometry and meta data of mouse immune profiling	FAIRDOMHub	https://fairdomhub.org/studies/927
Experimental models: Organisms/strains		
Mouse: Female C57Bl/6J	The Jackson Laboratory	Cat # 000664
Recombinant DNA		
pUC19 vector	New England Biolabs	Cat # N3041S
Software and algorithms		
Flow Jo version 10.8.1	BD Bioscience	https://www.flowjo.com
GraphPad Prism versions 9 to 10	GraphPad	https://www.graphpad.com
RStudio version 2021.09.0+351	CRAN	https://www.r-project.org
R version 4.0.3	CRAN	https://www.r-project.org
Seurat v4.0.0	Hao et al.[67]	https://github.com/satijalab/seurat
single cell cluster and analysis code	This paper	https://zenodo.org/records/6329999

EXPERIMENTAL MODEL AND STUDY PARTICIPANT DETAILS

Mice

C57BL/6 mice () were purchased from The Jackson Laboratory (Bar Harbor, ME). Mice were housed in specific-pathogen free BSL3 facilities of Harvard T.H. Chan School of public Health and/or the Ragon Institute of MGH, MIT, and Harvard for the duration of the experiment., C57BL/6 female mice aged 6 weeks were used for in vivo studies of antibody-mediated restriction; these mice were acclimated for 1 week in the animal facility prior to experimental procedures. Female mice between 6-8 weeks were used for bone marrow isolation and cell culture. All animal experiments were conducted in accordance with procedures approved by the Institutional Animal Care and Use Committees of Harvard T.H. Chan School of Public Health and the Ragon Institute of MGH. MIT, and Harvard.

Bone marrow derived dendritic cells, macrophages, and neutrophils

Bone marrow was isolated from female C57BL/6 mice, aged 6-8 weeks purchased from Jackson Laboratory. BMDC and neutrophils were generated in 7-day cultures with complete RPMI-10 supplemented with 15ng/mL recombinant GM-CSF (PeproTech). Cells from the floating fraction were harvested and BMDC were sorted using anti-CD11c MicroBeads (Miltenyi Biotech) or anti-Ly6G

MicroBeads (Miltenyi Biotech) for the isolation of BMDC and PMN, respectively. BMM were differentiated in complete DMEM-10 supplemented with 15 ng/mL recombinant M-CSF(PeproTech) and 7 days later adherent macrophages were collected from the culture dish with warm PBS. Cell phenotype was confirmed by antibody staining at the conclusion of the "*Mtb phagocytic assay*"; MHC II (BMDC), Ly6G (PMN), of CD11b+MHC II^{lo} (BMM). No additional authentication was performed of these primary mouse cells.

Bacterial Strains

YFP-expressing *M. tuberculosis* (courtesy of C. Sassetti) and its parental strain H37Rv (BEI Resources NR-123) were used for mouse aerosol infections. For *in vitro* infection of phagocytic cells YFP-*Mtb* was used to track bacterial uptake and *Mtb-276*, a luminescent *Mtb* strain generated with a modified form of pMV306hsp+LuxG13 (Addgene 26161) (*lux-Mtb*, from B. Bryson) was used to track bacterial growth in the *in vitro Mtb* restriction assays. *Mtb* cultures were grown to mid-log in Difco Middlebrook 7H9 media (Millipore Sigma) supplemented with 10% OADC (Millipore Sigma) and 0.05% Tween 80 and 37C shaking at 100 rpm. YFP-expressing Mtb were grown in the presence of the selection antibiotic hygromycin (50 μg/ mL) and lux-Mtb was cultured in Zeocin supplemented (20 μg/ mL) media. To count colony forming units, Mtb was palted on 7H11 agar plates (Millipore Sigma) supplemented with 10% OADC.

METHOD DETAILS

Aerosol infection of mice

7-week-old female C57BL/6 mice were injected with 100 μg of antibody (5 mg/kg) intraperitoneally (i.p.) one day prior to aerosol infection with YFP-H37Rv. Prior to infection H37Rv was cultured in 7H9-OADC media to mid-log phase and passaged once. Mice were inoculated with 50-200 CFU using an Inhalation Exposure Unit (Glas-Col). 3 animals from the aerosol infection were sacrificed one day following infection to determine the Day 1 CFU dose. 14 days following aerosol infection, all mice were sacrificed, and lungs and spleen were harvested for CFU plating on 7H11 Agar plates supplemented with 10% OADC (Millipore Sigma) and single cell suspensions were stained for flow cytometric analysis.

Antibody cloning and expression

Previously published VH/VL genes of monoclonal antibodies (A194,[28] D2,[11] 710 and 712,[27] MoAb1,[28] 2e9,[13] SMITB14,[9] and 24c5[68]) were cloned as human IgG1 Fc variants. Additional VH/VL sequences were courtesy of and MassBiologics and Chris Sassetti (OM- and CP- clones), AERAS/IAVI (Apa30), and BEI Resources (CS-90, a-Rv1411c, IT-15, Mpt64(B), KatG2, CS-35). Antibody VH/VL sequences were cloned together with hIgG1, mIg2a, mIgG2a N297A, and mIgG1 Fc sequences, and the corresponding antibodies were produced following transfection of plasmids into Expi293F cells (in the Dana Farber Cancer Institute Antibody Production Core). Antibodies were enriched from culture supernatants using protein G beads and were tested for endotoxin. Only antibody preparations with less than 0.5 endotoxin unit/mL detected were used in our experiments.

Mtb surface staining

10^7 YFP-*Mtb* cultured in 7H9 with and/or without 0.05% Tween-80, were combined with 1μg of mAb in a 96-well plate at 37°C for one hour. Following incubation with antibody, *Mtb* was washed 2x with PBS and stained with an αhuman IgG1-Fc antibody (M1310G05, Biolegend) secondary antibody. After staining with secondary antibody, *Mtb* was washed with PBS and fixed overnight with 4% paraformaldehyde (PFA) before analysis on a BD LSR Fortessa and High Throughput Screening (HTS) plate reader. Data were analyzed using FlowJo software version 10.8.1 for Mac OS X.

LAM coated bead phagocytic assays

Biotinylated LAM was generated by combining 100 μg of LAM (BEI Resources NR-14848) dissolved ddH_2O (1mg/mL), with 10 μL of 1M sodium acetate (NaOAc, Millipore Sigma) and 2.2 μL of 50mM sodium periodate ($NaIO_4$, Millipore Sigma); this solution was incubated for 60 minutes (mins) on ice in the dark to oxidize LAM. To stop the oxidation reaction, 12uL of 0.8M NaIO4 was added to the solution and incubated for 5mins at room temperature (RT) in the dark. The oxidized LAM was transferred to a fresh tube and combined with 10 μL 1M NaOAc and 22 μL of 50mM hydrazide biotin (Millipore Sigma), this was incubated at RT for 2 hours (hrs) to biotinylate LAM. The reaction mixture was buffer exchanged on an Amicon 3KDa cutoff 0.5mL Centrifuge column (Millipore Sigma) to remove excess biotin by washing 3 times with PBS. The buffer-exchanged biotinylated LAM was suspended in a final volume of 100 μL of PBS. As described,[18] biotinylated LAM was combined with 1 μm green fluorescent neutravidin beads (ThermoFisher) incubated overnight and washed to generate LAM-coated beads. These beads were co-incubated with 0.5 μg of αLAM Fc-variants for 1hr at 37°C to generate immune-complexes, washed with PBS then combined with either RAW cells for antibody-dependent phagocytosis (ADCP) assays or bone marrow derived neutrophils (generated as described below) for antibody-dependent neutrophil phagocytic (ADNP) assays. Cells and immune complexes were co-incubated for 1hr at 37°C, after which the cells were washed with PBS, stained with fixable live/dead NearIR stain (ThermoFisher), and fixed with 4%PFA. Phagocytosis data was collected on a BD LSR Fortessa and HTS plate reader. Data were analyzed using FlowJo software version 10.8.1 for Mac OS X. Phagocytic Scores were determined as (%Green *LAM-bead*$^+$Live Cells x MFI of *Bead*$^+$ Cells)/100 for each of the antibody conditions tested.

Mtb Phagocytic Assays in bone marrow derived cells

Differentiated cells were seeded into 96-well plates at $3x10^4$/well. $1.5x10^5$ antibody-coated *Mtb* (prepared as described above in *Mtb surface staining*) were added to each well. Cells and bacteria were co-incubated for phagocytosis for 1hr, after which extracellular bacteria were washed off with PBS and the cells were stained with CD11b and Live/Dead for identification of live cells via flow cytometry. Cells were fixed at 4°C overnight with 4% PFA and run on a BD LSR Fortessa and HTS plate reader. Data were analyzed using FlowJo software version 10.8.1 for Mac OS X. Phagocytic Scores were determined as (%Mtb^+Live Cells x MFI of Mtb^+ Cells)/100 for each of the antibody conditions tested.

IC50 determination for LAM mAbs

ELISA plates (ThermoFisher 269620 439454) were precoated with 100 μL PBS containing 2 μg/mL LAM overnight at 4°C. Plates were washed 5 times with PBS Tween 0.5% (PBST), blocked with 5% BSA for one hour at RT, and was again washed PBST 5 times before adding diluted mAb. Glycolipid-specific mAbs (SMITB14, MoAb1, CS-35, A194, OM2-L22, and CP2-R3, Table 1) at a starting concentration of 200 ng/mL were serially diluted 2-fold, and 9 dilutions per antibody were added to LAM-coated and pre-washed plates. Antibodies were incubated at RT for 2 hours before washing the plates and adding hIgG1 detection antibody (Bethyl Laboratory #A80-104P). Plates were incubated for 1 hour with secondary antibody and washed with PBST 5 times before adding TMB substrate (BD) to develop the signal. The reaction was stopped with 2N sulfuric acid and ELISA plates were read on a Tecan infinite M1000pro plate reader.

The collected O.D. values from the antibody dilution series in ELISA was used to calculate IC-50. Each mAb dilution was assayed in duplicate. The resulting dilution curve was plotted in GraphPad Prism and IC-50 was determined by fitting a nonlinear curve to the averaged data per mAb, which was constrained to a 0% baseline defined by the average O.D. of the non-specific human IgG1 isotype control antibody. $IC\text{-}50^{-1}$ are reported to demonstrate increased LAM-binding capacity of the mAbs relative to controls.

Luminex-based FcR-binding assay

LAM was covalently coupled to MagPlex Luminex beads as described[43] and these beads were combined with 10 ng of αLAM Fc-variants and incubated for 1hr at RT in a 96-well plate to form immune complexes that were then washed with PBS and probed for binding to mouse FcγR. To measure FcγR binding to these Fc-variant immune complexes, FcγR detectors were generated by biotinylating Avi-tagged mouse FcγRIIB, FcγRIIA, RcγRIV (generated by the Duke Human Vaccine Institute) and conjugating the biotinylated FcγR with Streptavidin-PE (Prozyme PJ31S).[69] FcR detectors were incubated with αLAM ICs, then washed and resuspended in BioRad Sheath Fluid. The MFI of FcγR-PE was detected for each condition on the FlexMap3D (Luminex).

Luminex-based complement deposition assay

LAM-coated Luminex beads as described in the FcR-binding assay above were incubated with 10 ng αLAM Fc-variants for 1 hr at RT to form immune complexes. In addition to LAM coated beads a BSA-coated control bead was spiked in for antigen-specificity control in each well. After washing 4 times with PBS-Tween 0.5%, immune complexes were incubated with Low-Tox Guinea Pig Complement (Cedar Lane labs) which was serially diluted five-fold in veroneal buffer (Millipore Sigma) ranging from 1:20 to 1:50,000. Complement and immune complexes were incubated for 30 minutes. Cells were washed 4 times with PBS-Tween 0.5%. And the complement-bound complexes were stained with anit-C3-FITC mouse sera (AP bio) diluted 1:1000 for 15 mins at RT in the dark. Complexes were washed 3x with PBS-Tween 0.5% and fixed with 4% PFA before running on a BD LSR Fortessa and HTS plate reader to detect anti-C3-FITC signal.

Flow staining of infected lungs

Single cell suspensions from Mtb-infected lungs were generated by digestion with 10mg/mL Type IV collagenase D (Worthington) and 30 μg/mL DNAseI (Roche) for 1hr at 37°C in a shaker. Cells were washed with PBS then stained for innate immune cells using viability dye (eBioscience Fixable Viability Dye eFluor455UV) and the fluorescently-labelled Abs BUV737-CD19 (1D3, BD), BUV395-CD45 (30-F11, BD), PerCp-CD11c (N418,Bioegend), BUV805-CD11b (M1/70), BV605-Ly6G (HK1.4, Biolegend), AlexaFluor700-Ly6C (1A8, Biolegend), Pacific Blue-IA-IE (M5/114.15.2, Biolegend), BV510-CD24 (M1/69, Biolegend), PE-Cy7-CD64 (X54-5/7.1 FC, Biolegend), BV711-CD16/32 (93, Biolegend), BV786-CD16.2 (9e9, Biolegend), and PE-CD351(TX61, Biolegend). Mtb-infected cells were identified by the expression of YFP. Lung cells were stained, washed with PBS, and fixed in 4% PFA overnight. The samples were analyzed on the BD FACSymphony™ A5 SE Cell Analyzer using BD TruCount (Cat# 340334) tubes to determine the total number of CD45+ cells in each sample; the cells and TruCount beads were collected on BD FACS Symphony and analyzed with FlowJo version 10.8.1 for Mac OS X. The gating strategy for immune cell identification is outlined in Figure S4.

Mtb restriction assay in sorted lung immune cells

Single cell suspensions were generated from lungs of naïve 6-week-old female C57Bl/6 mice and stained with antibodies as described in the methods used for flow cytometry of *Mtb*-infected lungs. AM, IM, and PMN were sorted from the lung suspension using the gating strategy outlined in Figure S3 on a BD FACS AriaFusion. The cells were resuspended in phenol-free complete RPMI-10 media without antibiotic and plated in 96-well plates (Greiner BioOne: #655083) and 10,000 AM, IM, and PMN were plated per well. At least five days prior to infection of these cells, H37Rv-276, a luciferase-expressing *Mtb* (lux-*Mtb*), was cultured in 7H9-OADC media to mid-log phase at 37°C and passaged once prior to infection. Bacteria was washed and resuspended in RMPI-10

without phenol and pre-coated with antibody as described above for *Mtb* surface staining. 1.5 x10^4 antibody-coated *Mtb* was added to 96-well plates containing previously aliquoted lung immune cells for an approximate MOI of 0.5. Luminescence readings were taken daily over the course of 192 hours (hr). Luminescent values were fold normalized to background signal captured in uninfected wells of the plate, and background-corrected luminescent values were reported as the fold change in lux-*Mtb* signal relative to the starting *Mtb* luminescence at the 0 hr time point of the assay. Area Under the Curve (AUC) values for each mAb treatment *Mtb* growth curve was calculated to quantify the difference the bacterial restriction mediated by mAb treatment.

Single-cell sorting and RNA Sequencing of mouse lung cells

6-week-old female C57Bl/6 mice were purchased from Jackson Laboratories and injected with PBS or 100 μg of aLAM-mIgG2a or -mIgG2a N297A (5 mg/kg) i.p. (3 mice/group) one day prior to aerosol infection (Biaera AeroMP-Hope aerosolization unit) with YFP-expressing H37Rv. On day 5 post infection, mice were sacrificed, and a single cell suspension of lungs cells was generated for flow sorting. Prior to sorting for CD45+ cells, samples were then quenched with FACS buffer (PBS with 2% FBS and 2 mM EDTA), washed once, and counted before proceeding with MULTI-seq barcoding. Samples were barcoded with 2.5 μM of MULTI-seq Lipid-Modified Oligos (LMO) (Millipore Sigma) anchor and barcode for 5 minutes on ice in PBS before adding 2.5 μM of the LMO co-anchor and incubating for an additional 5 minutes. Samples were quenched with 1% BSA in PBS and washed once with PBS before staining with the antibodies according to the above flow staining method. CD45+ cells were sorted on a BD FACS AriaFusion. Sorted cells were processed using the Chromium Single Cell 3' Reagent Kits (10X Genomics) per the manufacturer's protocol in 2 microfluidic lanes. Again, 0.5 U/μL RNase inhibitor (Roche) was added to the single-cell suspension and cDNA was heat-inactivated at 95°C for 15 minutes prior to BSL3 removal. Libraries were sequenced on a NextSeq500 (Illumina), and the data were aligned to the mm10 reference using Cell Ranger Count v6.0.1.

Analysis of infection scRNA-seq data

LMO barcode and gene expression count matrices were merged and analyzed using R (v4.0.3) and Seurat (v4.0.0). Samples were demuxed using HTODemux (Seurat). Data from both CD45+ and *Mtb*+ sorted samples were merged. Cells with less than 200 unique molecular identifiers (UMIs) counted and more than 25% mitochondrial UMIs were excluded. 3,000 variable features were used for Principal Component Analysis. Counts were normalized using the default parameters from NormalizeData (Seurat), i.e., scaling by 10,000 and log normalization. Walktrap (igraph) clustering was performed on the shared nearest neighbor graph generated from FindNeighbors (Seurat) using 20 principal components and k = 20. Cell type annotation was based on expert annotation and predicted cell type labels from the Tabula Muris dataset. Cell type labels were predicted using FindTransferAnchors, MappingScore, and TransferData (Seurat) with 20 dimensions and 20 trees. Myeloid cell types were subclustered separately by repeating the steps above on the cell subsets. Marker gene statistics were calculated using wilcoxauc (presto). The *in vivo* scRNA-seq data is accessible on GEO (GSE198064).

Gene Set Enrichment Analysis

A gene expression data set (or gene sets) for cells of the alveolar macrophage and neutrophil subclusters was extracted per mouse and pseudo-bulked. The pseudo-bulked data was used to perform pathway enrichment analysis comparing PBS-, mIgG2a-, and mIgG2a N297A-treated mice to the others (mIgG2a/PBS, mIgG2a/N297A, and N297A/PBS). GSEA software (version 4.2.1) was used to rank the genes expressed in AM from treated mice and calculate enrichment of genes in hallmark genes list curated by MSigDB.[70] Gene-sets enriched in either treatment group with a nominal p value < 0.05 were used for bubble plot visualization.

Data Analysis and Visualization

Univariate data visualization and statistical analysis were performed using GraphPad Prism (Version 9.3.1) and "ggplot" package in RStudio (version 2021.09.0+351).

QUANTIFICATION AND STATISTICAL ANALYSIS

The code utilized for the subclustering and analysis of the scRNAseq data is depositied on Zenodo https://doi.org/10.5281/zenodo.6329999.